JOC The Journal of Organic Chemistry

Article

pubs.acs.org/joc

Excited-State Intramolecular Proton Transfer Molecules Bearing *o*-Hydroxy Analogues of Green Fluorescent Protein Chromophore

Wei-Ti Chuang,[†] Cheng-Chih Hsieh,[†] Chin-Hung Lai,[†] Cheng-Hsuan Lai,[†] Chun-Wei Shih,[†] Kew-Yu Chen,*[,‡] Wen-Yi Hung,*[,§] Yu-Hsiang Hsu,[§] and Pi-Tai Chou*[,†]

[†]Department of Chemistry, National Taiwan University, Taipei 106, Taiwan, Republic of China

[‡]Department of Chemical Engineering, Feng Chia University, Taichung 40724, Taiwan, Republic of China

[§]Institute of Optoelectronic Sciences, National Taiwan Ocean University, Keelung 202, Taiwan, Republic of China

Supporting Information

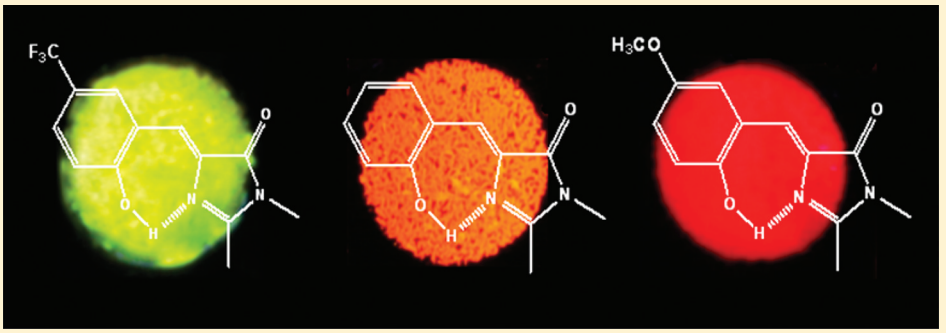

ABSTRACT: *o*-Hydroxy analogues, **1a**–**g**, of the green fluorescent protein chromophore have been synthesized. Their structures and electronic properties were investigated by X-ray single-crystal analyses, electrochemistry, and luminescence properties. In solid and nonpolar solvents **1a**–**g** exist mainly as *Z* conformers that possess a seven-membered-ring hydrogen bond and undergo excited-state intramolecular proton transfer (ESIPT) reactions, resulting in a proton-transfer tautomer emission. Fluorescence upconversion dynamics have revealed a coherent type of ESIPT, followed by a fast vibrational/solvent relaxation (<1 ps) to a twisted (regarding exo-C(5)–C(4)–C(3) bonds) conformation, from which a fast population decay of a few to several tens of picoseconds was resolved in cyclohexane. Accordingly, the proton-transfer tautomer emission intensity is moderate (0.08 in **1e**) to weak ($\sim 10^{-4}$ in **1a**) in cyclohexane. The stronger intramolecular hydrogen bonding in **1g** suppresses the rotation of the aryl–alkene bond, resulting in a high yield of tautomer emission ($\Phi_f \approx 0.2$). In the solid state, due to the inhibition of exo-C(5)–C(4)–C(3) rotation, intense tautomer emission with a quantum yield of 0.1–0.9 was obtained for **1a**–**g**. Depending on the electronic donor or acceptor strength of the substituent in either the HOMO or LUMO site, a broad tuning range of the emission from 560 (**1g**) to 670 nm (**1a**) has been achieved.

1. INTRODUCTION

Green fluorescent protein (GFP)[1] has received intense attention because of its ubiquitous applications in molecular biology and biochemistry. GFP takes advantage of the presence of a chromophore, (*Z*)-4-(4-hydroxybenzylidene)-1,2-dimethyl-1*H*-imidazol-5(4*H*)-one (*p*-HBDI; see Scheme 1), which undergoes excited-state proton transfer (ESPT)[2] via the proton relay of the water network and/or some residues to a remote residue such as E222,[3] resulting in a very intense anion fluorescence. From a chemistry point of view, most of the research has focused on the chemical modification of *p*-HBDI[4] analogues at the C(1) position (see Scheme 1), such that the emission color can be tuned via the substituent effect.[5] Studies nevertheless reveal a cutoff in properties between wild type GFP (or certain GFP mutants) and the synthetic analogue chromophores of *p*-HBDI. The GFP-free *p*-HBDI gives virtually no emission in fluid solution at room temperature. The results suggest an effective radiationless transition operating in *p*-HBDI, plausibly induced by conformational relaxation along torsional deformation[6] of the two exocyclic C–C bonds from the initially prepared Franck–Condon state to a nonfluorescent twisted intermediate.[7] The shallow potential energy surface of the intermediates may conically intersect with

Scheme 1. Structural Isomers of *p*-HBDI and *o*-HBDI

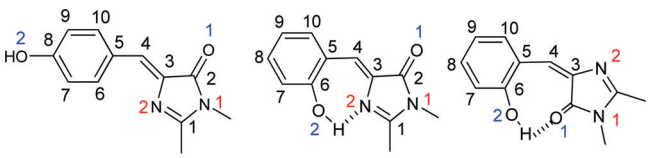

Received: June 27, 2011
Published: September 26, 2011

Scheme 2. (A) Synthetic Route of *o*-Hydroxy Analogues (1a–g) of the Green Fluorescent Protein Chromophore and (B) Synthesis of *Z* and *E* Forms of 4-((1*H*-Pyrrol-2-yl)methylene)-1-methyl-2-phenyl-1*H*-imidazol-5(4*H*)-one (1h)

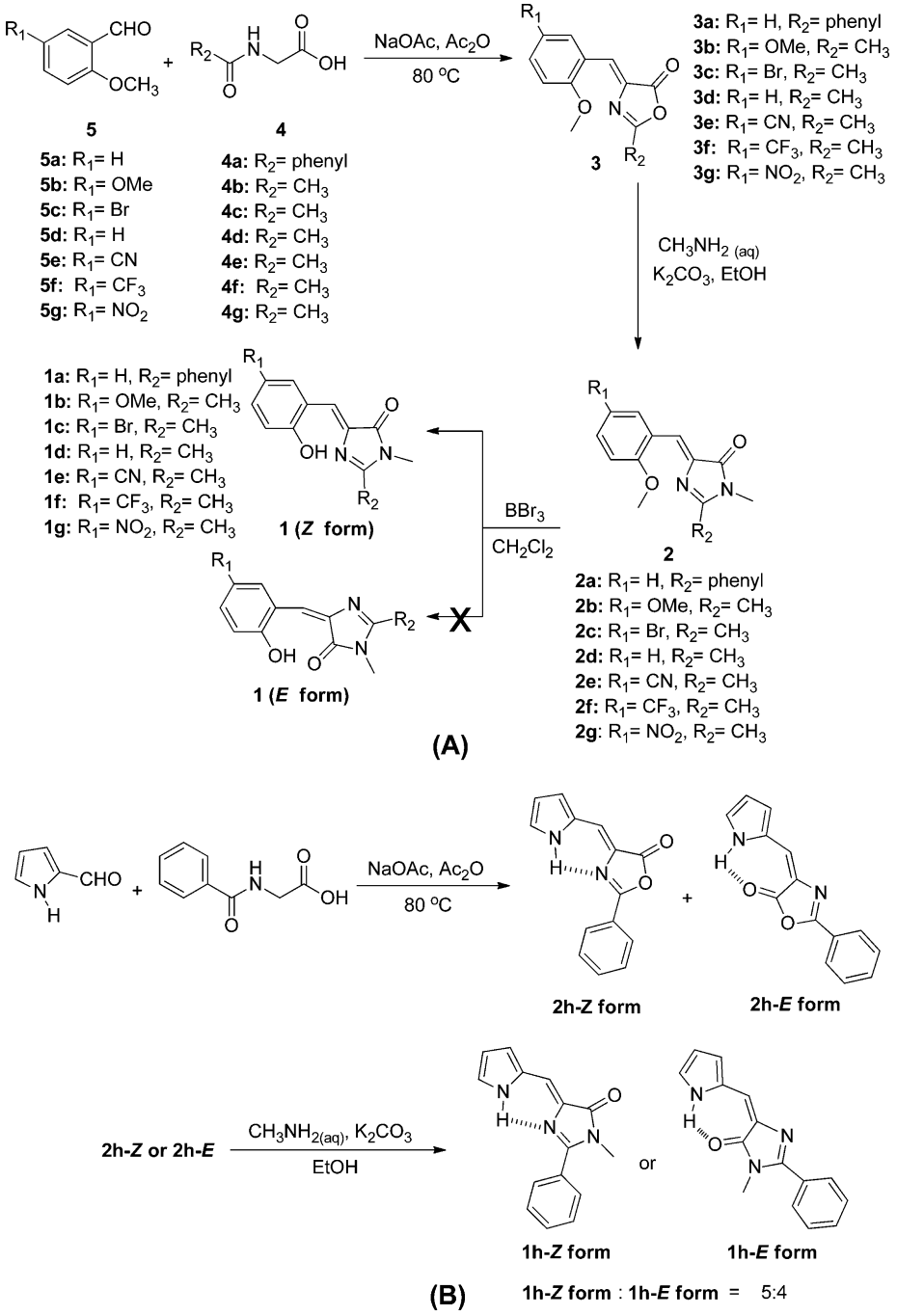

that of the ground state, inducing the dominant radiationless deactivation.[8] Such a conformational relaxation is greatly suppressed in wild GFP by its proton relay network, forming a rigid environment to restrain the conformational relaxation.

Recently, with an aim to probe the associated excited-state proton transfer phenomena, two research groups have made different approaches via switching the position of the hydroxyl group in *p*-HBDI. On the one hand, Tolbert and co-workers have developed a promising strategy toward the *m*-GFP chromophore,[9] *m*-HBDI, to probe a stepwise proton transfer mechanism in protic solvents. The results serve as a paradigm for the elementary proton transfer steps in relevant systems. On the other hand, we have strategically designed and synthesized an *o*-GFP chromophore, *o*-HBDI (see Scheme 1).[10] *o*-HBDI possesses a seven-membered-ring hydrogen bond, from which the excited-state intramolecular proton transfer (ESIPT) takes place, resulting in a remarkable proton transfer tautomer emission of ~605 nm in organic solvents such as cyclohexane. ESIPT also takes place in the solid film, giving rise to a ~595 nm tautomer emission with a quantum yield as high as 0.4. While applications of *o*-HBDI are pending exploration, it is believed that the chemical derivation as well as the associated chemical and photophysical properties can be further explored. In view of the photophysical properties, we have recently performed comprehensive studies of *o*-HBDI during an overall proton transfer cycle. The results conclude that ESIPT in *o*-

dx.doi.org/10.1021/jo2012384 | *J. Org. Chem.* 2011, 76, 8189–8202

Scheme 3. Proposed Mechanism

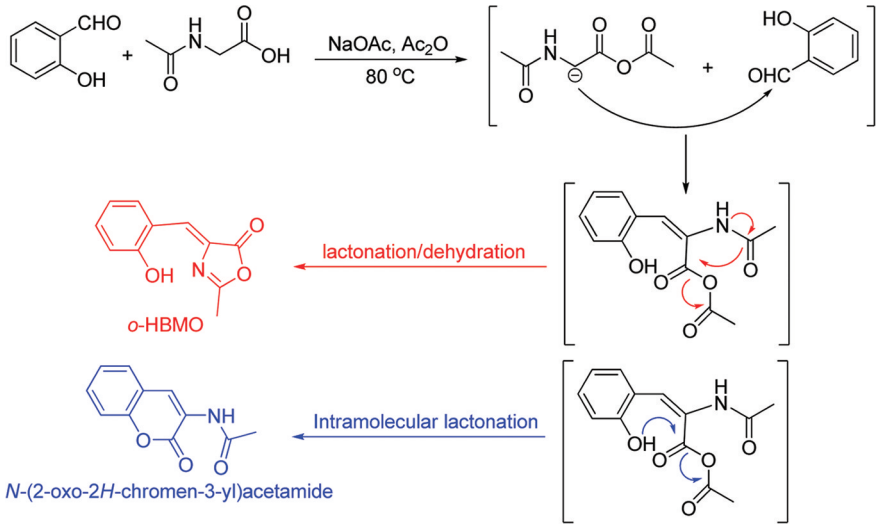

HBDI is essentially triggered by low-frequency motions associated with hydrogen bonding and may be barrierless along the reaction coordinate. Femtosecond UV−vis transient absorption and IR spectra also provide supplementary evidence for the structural evolution during the reaction.[11]

From the viewpoint of chemical derivation, in this study, we have made intense efforts to carry out the chemical derivatization of *o*-HBDI. Our aim is twofold. First, we plan to systematically study the synthetic routes and the associated reaction mechanism. Second, on the basis of this series of ESIPT molecules we will be able to gain more insight into the relationship for the photophysical behavior versus structural properties. We also expect that, through the synthetic approach, it is feasible to fine-tune the proton transfer tautomer emission covering a broad spectral range from visible to near-IR, establishing a new class of *o*-GFP dyes. Finally, the successful fabrication of OLEDs using *o*-HBDI provides a new perspective of utilizing proton transfer dyes in electroluminescence devices.

2. RESULTS AND DISCUSSION

2.1. Design Strategy. A preliminary result of the computational approach for *o*-HBDI[10] indicated that the frontier orbitals contributing to $S_0 \rightarrow S_1$ as well as $S_0' \rightarrow S_1'$ (the prime denotes the proton-transfer tautomer) transitions in the normal and proton-transfer tautomer species, respectively, can be mainly ascribed to *o-hydroxyl* phenyl ring (HOMO) and imidazolone (LUMO) moieties. On this basis, a series of derivatives of *o*-HBDI (hereafter, *o*-HBDI is denoted as **1d** in this study), **1a**−**g**, can be strategically designed by functionalizing different substituents at the R_1 or R_2 position (see Scheme 2A).

Via alteration of the electron donating/withdrawing strength or extension of π-conjugation of the substituent, the correlation among molecular structure, hydrogen-bonding strength, and the corresponding ESIPT properties can be systematically probed. The interplay between HOMO and LUMO energy levels should fine-tune the energy gap of proton-transfer tautomer emission covering a broad spectral range. To probe the hydrogen bond−geometry relationship, we also took one more step via replacing the phenol ring in **1a** by the pyrrolic moiety, forming **1h** (see Scheme 2B). Details of synthesis, characterization, and the associated chemical, electrochemical, and ESIPT properties are elaborated in the following sections.

2.2. Synthesis and Characterization. Similar to the preparation of *p*-HBDI and its analogues,[8] in our earlier attempt, we expected that *o*-HBDI (**1d**) and the corresponding analogues might be synthesized via the reaction of *o*-hydroxybenzaldehyde (see Scheme 3) with *N*-acetylglycine in the presence of acetic anhydride and sodium acetate. However, the intermediate (4*Z*)-4-(2-hydroxybenzylidene)-2-methyloxazol-5(4*H*)-one (*o*-HBMO; see Scheme 3) obtained from the reaction between *N*-acetylglycine and *o*-hydroxybenzaldehyde was obtained in a poor yield of <20%. Instead, as shown in Scheme 3, a substantial amount of *N*-(2-oxo-2*H*-chromen-3-yl)acetamide was isolated and identified by X-ray single-crystal analyses (see Figure S47 in the Supporting Information).

In view of the mechanistic approach, we propose that the presence of the *o*-hydroxyl group plays a key role in the observed reaction pattern. In basic solution, the phenolate acts as a nucleophile to attack the carbonyl oxygen, resulting in a cyclization reaction. A similarly low yield (<20%) of intermediates, i.e. derivatives of *o*-HBMO, was obtained when various *o*-hydroxybenzaldehyde derivatives were used as starting reactants. As a result, the subsequent workup procedure by treating methylamine in the presence of K_2CO_3-basified ethanol, followed by neutralization, gave the corresponding *o*-HBDI derivatives **1a**−**g** in a poor yield of <10%.

Alternatively, a more effective synthetic route to achieve the substituted *o*-HBDI (**1a**−**g**) began with *o*-methoxybenzaldehyde or its derivatives (see Scheme 2A). The lack of an *o*-hydroxyl group and hence the intramolecular lactonation leads to the formation of **3a**−**g** in a good yield of 71−76%. Subsequent reaction of **3a**−**g** with methylamine, followed by deprotection of the methyl group of **2a**−**g** by BBr_3, afforded **1a**−**g** in an overall product yield of >40%. Detailed synthetic procedures as well as ^{1}H NMR, ^{13}C NMR, MS, and HRMS data are provided in the Experimental Section. It is also worth noting that treatment of **2b** with BBr_3 (4 equiv, 0 °C, 4 h) resulted in cleavage of the methyl ether group only at the C(6) position (see Scheme 1 for numbering), giving **1b** in 89% yield. The high regioselectivity of **2b** with BBr_3 can be rationalized by the combination of two key factors. Chelation of the imine nitrogen and the ether oxygen to the electron-deficient BBr_3 is

dx.doi.org/10.1021/jo2012384 | J. Org. Chem. 2011, 76, 8189−8202

expected to be thermally favorable, forming the intermediate **ImA** shown in Scheme 4. Moreover, in comparison to the

Scheme 4. Proposed Mechanism

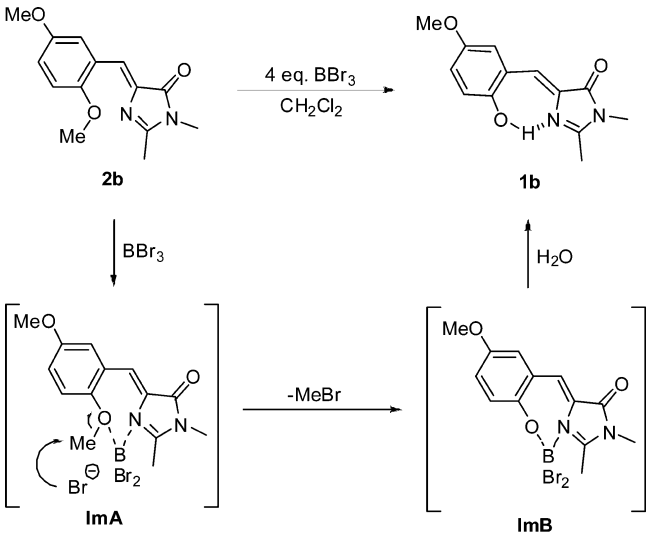

phenolate moiety at the C(9) position, *o*-phenolate is considered to be a better leaving group, due to the resonance effect that weakens the O−CH_3 bond. Accordingly, the chelation exerts a regiodirective bias and results in the subsequent cleavage of the methyl ether at the ortho position (intermediate **ImB**; see Scheme 4).

The dominance of a *Z* isomer for **1a−g**, namely intramolecular hydrogen-bond formation between O(2)−H and N(2), is firmly supported by a combination of ^{1}H NMR and X-ray single-crystal analyses. In the ^{1}H NMR studies, the existence of a strong hydrogen bond between O(2)−H and N(2) is evidenced by the observation of a large downfield shift of the proton peak at δ >13 ppm for all compounds **1a−g**, the values of which are in the order **1g** (15.11 ppm) > **1e** (14.70 ppm) > **1f** (14.18 ppm) > **1a** (13.94 ppm) > **1c** (13.82 ppm) > **1d** (13.68 ppm) > **1b** (13.26 ppm) in dry CD_2Cl_2. For the C(9) position substituents (R_1; see Scheme 2) that are in para positions with respect to the hydroxyl group, the trend of the O−H proton peak of **1g** > **1e** > **1f** > **1c** > **1d** > **1b** is in good correlation with the associated electron-withdrawing strength of **1g** (−NO_2) > **1e** (−CN) > **1f** (−CF_3) > **1c** (−Br) > **1d** (−H) > **1b** (−OCH_3), in which OCH_3 in **1b** is an electron-donating group. If we assume that the chemical shift of the hydroxyl proton in **1a−g** belongs to the class of aromatic alcohols, the hydrogen bonding energy, ΔE in kcal/mol, can be empirically estimated by introducing Shaefer's correlation,[6] expressed as

$$\Delta\delta = (-0.4 \pm 0.2) + \Delta E \qquad (1)$$

where $\Delta\delta$ is given in parts per million for the difference between chemical shift of the O−H peak of **1a−g** and that of phenol (δ 4.29).[6] Accordingly, the hydrogen-bonding energy is estimated to be **1g** (11.22 ± 0.2 kcal/mol) > **1e** (10.81 ± 0.2 kcal/mol) > **1f** (10.28 ± 0.2 kcal/mol) > **1a** (10.04 ± 0.2 kcal/mol) > **1c** (9.92 ± 0.2 kcal/mol) > **1d** (9.78 ± 0.2 kcal/mol) > **1b** (9.36 ± 0.2 kcal/mol). Although these values may be overestimated due to the use of an intermolecular hydrogen-bonding model (i.e., eq 1) for aromatic alcohols instead of a intramolecular model (**1a−g**), the trend of an increase in the hydrogen-bonding strength upon an increase of the electron-withdrawing substituent at the para position is evident. The results clearly follow a trend in that an increase of the acidity of the hydroxyl proton renders an increase of the intramolecular hydrogen bonding strength. Note that the substitution of CH_3 in **1d** by a phenyl ring at the C(1) position (Scheme 1, also see R_2 in Scheme 2), forming **1a**, seems to increase the basicity of the proton acceptor, i.e. the N(2) atom, through the resonance effect. As a result, **1a** exhibits a larger downfield shift of the O−H proton and hence a stronger hydrogen bond relative to **1d**.

Further support of the above assignments is given by the X-ray single-crystal analyses. Except for **1f**, growth of single crystals was successful for all compounds **1a−g** and their associated structures have been resolved by X-ray analyses. Using **1a** as a prototype, Figure 1A depicts the X-ray-resolved

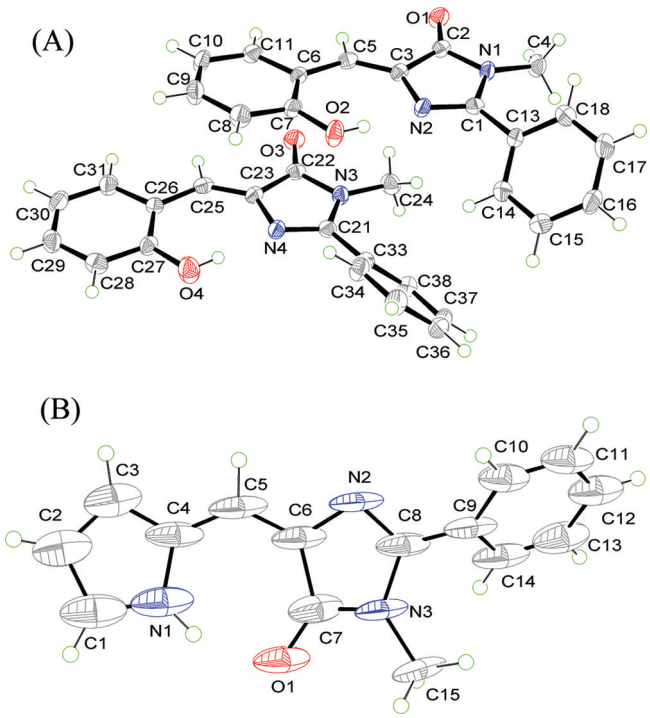

Figure 1. Molecular structures of (A) **1a** and its intermolecular relationship and (B) **1h-*E***. Thermal ellipsoids are drawn at the 50% probability level.

structure to address its salient featured, while the structures of **1b−e,g** are provided in the Supporting Information (see Figures S49−S53). First of all, according to the single-crystal structure, **1a−g** all reveal a *Z* configuration, in which the O−H proton is hydrogen-bonded with the N(2) nitrogen (see Scheme 1). Apparently, the results of X-ray analyses all indicate a short distance of <2.65 Å between O(2) and N(2) for **1a−e,g**, supporting the formation of an O(2)−H- - -N(2) intramolecular hydrogen bond. Moreover, with the exception of **1b** (2.588 Å), where resonance effects pertaining to the methoxy group may dominate the hydrogen-bonding character rather than inductive effects, the distance between O(2) and N(2) along the O(2)-H- - -N(2) hydrogen bond is in the order of **1d** (2.630 Å) > **1a** (2.610 Å) ≈ **1c** (2.608 Å) > **1e** (2.591 Å) > **1g** (2.579 Å), consistent with the hydrogen-bonding strength estimated from ^{1}H NMR measurements (vide supra). We will elaborate in the following and later sections that the hydrogen-bonding strength plays a role in accounting for the structure versus luminescence relationship.

dx.doi.org/10.1021/jo2012384 | *J. Org. Chem.* 2011, 76, 8189−8202

As for **1a**, evidenced by the dihedral angle ∠N(2)−C(3)−C(5)−C(6) = −2.39°, the X-ray structure reveals a planar configuration between the phenol and imidazolidinone rings. This, together with the distance O(2)−N(2) = 2.61 Å and ∠N(2)−H−O(2) = 175°, strongly supports a planar, seven-membered-ring intramolecular hydrogen-bond formation. Similar planar structures between phenol and imidazolidinone rings were obtained for compounds **1b**−**e**,**g** (see the Supporting Information). Although we did not obtain an X-ray structure for **1f**, it is reasonable to assume a similar molecular planarity. For **1a**, however, the phenyl substituent at the C(1) position was tilted by an angle of ∼37.9° with respect to imidazolidinone (see Figure 1).

Despite a planar molecular geometry, **1a**−**g** all revealed no notable intermolecular $\pi\cdots\pi$ contacts in the solid crystal. For example, **1a** appears to possess an alternating slab in the molecular packing and the distance between two adjacent phenol rings, estimated by the C(6)−C(26) distance, is 5.07 Å, while the distance between phenol (e.g., C(26)) and the imidazolidinone (C(2)) is estimated to be 3.3 Å. The lack of strong intermolecular π interactions is also supported by similar spectral features of the proton-transfer emission for **1a**−**g** in both solution and the solid phase (vide infra). The weak $\pi-\pi$ interaction could be due to the alternating slabs and lack of full π electron delocalization exerted between the phenol and imidazolidinone moieties.

The lack of an *E* isomer for **1a**−**g**, i.e. the formation of a C(2)═O(1)···H−O(2) eight-membered-ring hydrogen-bonding configuration, is of fundamental interest, which may be attributed to two possible factors. (1) The C(2)═O(1) carbonyl group is less basic than the N(2) nitrogen and hence forms weaker hydrogen bonds with respect to the −O(2)H proton. (2) The C═O(1)···H−O(2) eight-membered-ring hydrogen-bonded configuration (*E* form) is sterically hindered and hence is thermally unfavorable (see Scheme 1 for the *Z* and *E* forms). To verify these viewpoints, we then intentionally replaced the phenol by a pyrrolic moiety in **1a** and successfully synthesized the compounds 4-((1*H*-pyrrol-2-yl)methylene)-1-methyl-2-phenyl-1*H*-imidazol-5(4*H*)-one as both *E* (**1h-*E***) and *Z* (**1h-*Z***) isomers, which could be further separated via column chromatography (see Scheme 2B and Figure S54 in the Supporting Information). The assignment of each isomer can be preliminarily supported by ^{1}H NMR of the olefinic hydrogen. It has been reported that the olefinic hydrogen atom on the *cis*-N═C−C_6H_5 type of moiety is further downfield than that of the trans olefinic hydrogen.[12] Accordingly, **1h** with olefinic hydrogen peaks at 7.37 and 7.18 ppm (see Figures S43 and S45 in the Supporting Information) is assigned to be the *E* form (**1h-*E***) and *Z* form (**1h-*Z***), respectively. As a result, the ratio **1h-*E*:1h-*Z*** is calculated to be 4:5. As indicated by two downfield-shifted proton peaks of 13.21 ppm (**1h-*E***) and 11.12 ppm (**1h-*Z***) in CD_2Cl_2, the formation of seven- and six-membered hydrogen bonds is evident in **1h-*E*** and **1h-*Z***, respectively. Interestingly, due to the geometry fit, the *E* form having a seven-membered-ring N−H···O═< hydrogen bond seems to be stronger than the *Z* form possessing a six-membered-ring N−H···N hydrogen bond. The structure of **1h-*E*** was further confirmed by single-crystal X-ray diffraction analysis. As depicted in Figure 1B, the nearly planar configuration between pyrrole and imidazolidinone rings was established by ∠N(1)−H(1)−O(1)−C(7) = −0.43° and ∠N(1)−C(4)−C(6)−C(7) = −0.39°. This, together with the distance O(1)−H(1) = 1.71 Å and angle ∠N(1)−H(1)−O(1) = 147°, strongly supports the strong seven-membered-ring intramolecular hydrogen-bonding formation.

In a computational approach based on the B3LYP/6-31g(d,p) method incorporating solvation (PCM model in cyclohexane; see the Experimental Section), the **1h-*E*** form is calculated to be more stable than **1h-*Z*** by 1.08 kcal/mol, consistent with the experimental observation. With the same theoretical level and basis sets, we also performed the calculation of relative energy between the *Z* (seven-membered-ring) and *E* (eight-membered-ring) forms for *o*-HBDI (**1d**). The results show that the **1d-*Z*** form is more stable than the **1d-*E*** form by as much as 7.05 kcal/mol. Moreover, as for the **1d-*E*** form, the dihedral angles for C(4)−C(5)−C(6)−O(2) and C(3)−C(4)−C(5)−C(6) are calculated to be 42.3 and −24.8°, respectively, indicating a nonplanar structure. Evidently, for **1a**−**g** the eight-membered-ring hydrogen bond imposes a steric hindrance. The combination of these results leads us to conclude that steric effects play an important role regarding seven- versus eight-membered-ring hydrogen-bond formation for the **1a**−**g**.

2.3. Photophysical Properties. Figure 2A shows the absorption and emission spectra of **1a**−**g** in cyclohexane, while the pertinent photophysical data are given in Table 1. The absorption spectra are characterized by a low-lying band maximized at 380 nm (**1g**)−415 nm (**1a**), the ε values for which above 1.5×10^4 M^{-1} cm^{-1} make their assignments to the $\pi \rightarrow \pi^*$ transition unambiguous. In comparison to the absorption spectra of the corresponding methoxyl derivatives, i.e. **2a**−**g** (see Figure 2B), the absorption peak wavelengths in **1a**−**g** are obviously red-shifted, indicating that the formation of a O(2)−H···N(2) intramolecular hydrogen bond induces further π-electron delocalization and hence a smaller S_0-S_1 energy gap.

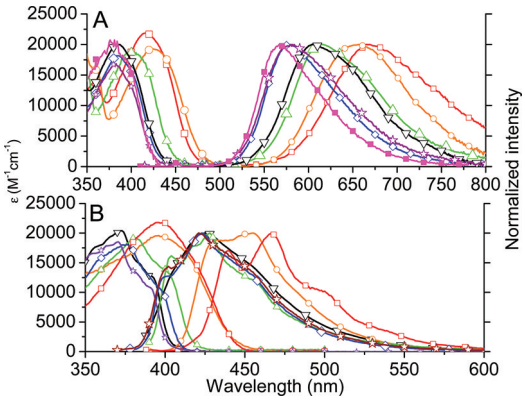

Figure 2. Absorption and emission spectra in terms of absorption extinction coefficient and the normalized emission spectra in cyclohexane: (A) **1a** (red □), **1b** (orange ○), **1c** (green △), **1d** (black ▽), **1e** (blue ◇), **1f** (brown ☆), and **1g** (magenta ■) in cyclohexane; (B) **2a** (red □), **2b** (orange ○), **2c** (green △), **2d** (black ▽), **2e** (blue ◇), and **2f** (brown ☆).

As for the steady-state emission, **1a**−**g** all exhibit solely an anomalously long wavelength emission (>550 nm) in cyclohexane. Figure 2A clearly shows a large separation of the energy gap between the 0−0 onset of the absorption and emission. The Stokes shift of the emission, defined by peak (absorption)-to-peak (emission) gap in terms of frequency, is calculated to be >8000 cm^{-1} for **1a**−**g**. To further verify the origin of the

dx.doi.org/10.1021/jo2012384 | J. Org. Chem. 2011, 76, 8189−8202

Table 1. Photophysical Properties of 1a–g and Their Methoxy Derivatives 2a–g

	solvent	λ_{abs} (nm)	λ_{em} (nm)	relaxation dynamics (ps)[a]	Φ ($\times10^{-3}$)		solvent	λ_{abs} (nm)	λ_{em} (nm)	relaxation dynamics (ps)	Φ ($\times10^{-3}$)
1a	C_6H_{12}	415	670	τ_1 = 0.07 (0.41)[b] τ_2 = 3.7 (0.59)	0.08	**1d**	C_6H_{12}	385	605	τ_1 = 0.11 (0.12) τ_2 = 31.9 (0.88)	3.1
	CH_2Cl_2	413	660	τ_1 = 0.10 (0.47) τ_2 = 3.0 (0.53)	0.11		CH_2Cl_2	386	603	τ_1 = 0.26 (0.23) τ_2 = 16.6 (0.77)	2.2
	CH_3CN	410	645	τ_1 = 0.49 (0.52) τ_2 = 2.4 (0.48)	0.17		CH_3CN	383	602	τ_1 = 0.39 (0.27) τ_2 = 7.8 (0.73)	1.5
2a	C_6H_{12}	390	465	τ_1 = 0.14 (0.13) τ_2 = 30.7 (0.87)	7.3	**2d**	C_6H_{12}	372	425	τ_1 = 0.63 (0.55) τ_2 = 4.1 (0.45)	0.5
1b	C_6H_{12}	425	655	τ_1 = 0.18 (0.29) τ_2 = 8.8 (0.71)	0.35	**1e**	C_6H_{12}	385	578	τ_1 = 0.71 (0.03) τ_2 = 835 (0.97)	80
	CH_2Cl_2	420	660		0.28		CH_2Cl_2	382	578	τ_1 = 0.47 (0.13) τ_2 = 177 (0.87)	20
	CH_3CN	410	645		1.6		CH_3CN	380	570	τ_1 = 0.14 (0.31) τ = 20.9 (0.69)	3.1
2b	C_6H_{12}	395	455	τ_1 = 1.3 (0.02) τ_2 = 339 (0.98)	64	**2e**	C_6H_{12}	373	423	τ_1 = 0.40 (0.34) τ_2 = 6.7 (0.66)	24
1c	C_6H_{12}	400	610	τ_1 = 0.72 (0.06) τ_2 = 81.4 (0.94)	4.6	**1f**	C_6H_{12}	383	575	τ_1 = 0.85 (0.07) τ_2 = 247 (0.93)	20
	CH_2Cl_2	397	615	τ_1 = 0.22 (0.23) τ_2 = 35.4 (0.77)	2.1		CH_2Cl_2	380	573	τ_1 = 0.32 (0.09) τ_2 = 66.8 (0.91)	5
	CH_3CN	390	625	τ_1 = 0.19 (0.26) τ_2 = 14.3 (0.74)	1.1		CH_3CN	376	570	τ_1 = 0.43 (0.25) τ_2 = 17.0 (0.75)	1.2
2c	C_6H_{12}	380	440	τ_1 = 0.24 (0.27) τ_2 = 28.6 (0.73)	9.2	**2f**	C_6H_{12}	370	422	τ_1 = 0.21 (0.10) τ_2 = 30.4 (0.90)	10
						1g	C_6H_{12}	380	567	τ = 2000	123
							CH_2Cl_2	382	570	τ = 620	57

[a]The relaxation dynamics pumped at 400 nm and monitored at the emission peak maximum. [b]Data in parentheses indicate the fitted pre-exponential factor, which was normalized to 1. For **1b** in polar solvents, please see the text for explanation.

emission, the methoxy derivatives of **1a–g**, i.e. **2a–g** (see Scheme 2), were also investigated. Owing to their lack of a hydroxyl proton, **2a–g** serve as models to represent the prohibition of the proton transfer reaction. As depicted in Figure 2B, for **2a–g**, the $S_0 \rightarrow S_1$ absorption versus the corresponding emission features reveals a good mirror image with a normal peak-to-peak Stokes shift of <4000 cm^{-1}. Accordingly, the assignment of ~560–670 nm emission for **1a–g** in cyclohexane to a proton-transfer tautomer emission is unambiguous, and ESIPT takes place from the phenolic proton (O(2)–H) to the N(2) nitrogen, forming the zwitterionic species depicted in Scheme 5. The lack of any normal emission

Scheme 5

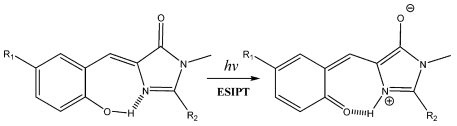

for **1a–g** in a steady-state manner indicates that the rate of ESIPT must be ultrafast, as evidenced by the recent study of **1d**[11] and the reaction dynamics of the rest of the title compounds elaborated in the next section.

Also, interestingly, despite the formation of an intramolecular hydrogen bond, ESIPT is prohibited in both **1h-*E*** and **1h-*Z*** forms, as indicated by the normal Stokes-shifted emission λ_{max} 470–480 nm with respect to the absorption peak: 410 nm for **1h-*Z*** and 415 nm for **1h-*E*** (see Figure 3), while no proton transfer emission can be resolved. Though it is pending a

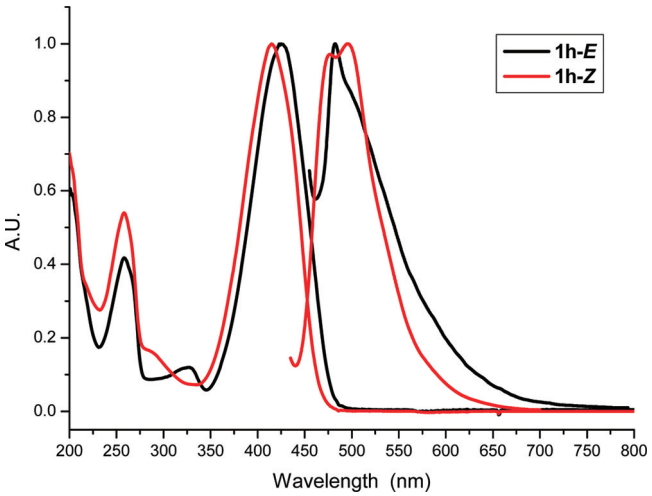

Figure 3. Absorption and emission spectra of **1h-*E*** (black) and **1h-*Z*** (red).

definitive explanation, we tentatively propose that the prohibition of ESIPT in **1h** might be due to the weakening of acidity at the pyrrolic hydrogen. We will have more discussion on this in section 2.5.

2.4. ESIPT and Relaxation Dynamics. The relaxation dynamics of **1a–g** have been measured with the femtosecond fluorescence upconversion in combination with time-correlated single photon counting techniques in various aprotic solvents. For the representative data, the best fitted time constants of the relaxation dynamics monitored at near the peak of the emission

dx.doi.org/10.1021/jo2012384 | J. Org. Chem. 2011, 76, 8189–8202

are given in Table 1. A fast time-resolved profile (<10 ps) using **1f** as a prototype in cyclohexane is depicted in Figure 4.

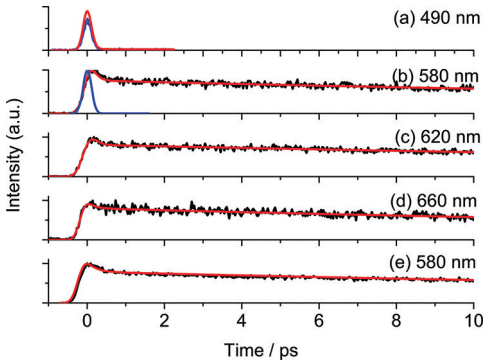

Figure 4. Fluorescence decay (black) and theoretical fitting (red) of **1f** at (a) 490 nm and (b) 580 nm, cross-correlation traces between the excitation and the gate pulse (blue) at (c) 620 nm and (d) 660 nm, and (e) deuterium substitution decay dynamics at 580 nm recorded in cyclohexane. The excitation wavelength was set to be 400 nm.

Upon monitoring at the region of e.g. 490 nm, presumably ascribed to the normal emission that could not be resolved by steady-state means, the upconversion signal consists of very fast rise and decay dynamics. For comparison, an experimental trace of the pump (400 nm) and gate (800 nm) cross-correlation function was also shown in Figure 4, which gives an fwhm of a Gaussian shape-like response profile of ~180 fs and within experimental error is indistinguishable with that obtained from the 490 nm upconversion signal. Figure 4 also reveals the time-dependent upconversion signal of the tautomer emission for **1f** as a function of the monitored emission wavelengths of >550 nm.

In general, independent of the monitored wavelength, the temporal resolution of the tautomer emission consists of both ultrafast rise and decay components, i.e. a spike, the shape of which is indistinguishable from that obtained from e.g. 385 (pump) and 770 nm (gate) cross-correlation functions (not shown here), followed by a small decay component of ~0.9 ps and a population decay time of 10 ps. The population decay time was further resolved to be 247 ps in cyclohexane by time-correlated single photon counting techniques. The population decay is strongly solvent dependent: 67 ps in CH_2Cl_2 and 18 ps in CH_3CN (see Table 1). Similar relaxation patterns, i.e. consisting of a spike, an ~1 ps decay component, and a population decay of several tens of picoseconds, are resolved for other title compounds upon monitoring at the peak of the tautomer emission. Using an ultrashort pulse (25 fs) excitation, our recent time-resolved studies of *o*-HBDI (**1d**)[11] have concluded that the spike can be further resolved, which shows a coherent vibration motion of low-frequency bending vibrations associated with hydrogen bonds. The ultrafast (25 fs) fluorescence upconversion experiments of **1a**–**g** are not relevant to the goals of this study, and the results will be published elsewhere. Also, as indicated by the only slight solvent polarity dependent shift of the emission spectra, the charge transfer character of tautomer emission for these *o*-HBDI derivatives is slim. This has been observed and discussed for compound **1d** in our recent report.[11] In another example, the emission peak wavelength of **1f** is measured to be 575 and 570 nm in cyclohexane and acetonitrile, respectively. Such a small and even slightly blue shift of the emission maximum indicates that the excited state charge transfer character is rather small or even negligible. Thus, dynamic Stokes shifts should not play a role in the observed relaxation dynamics of the title compounds. Accordingly, the common ~1 ps decay component is attributed to vibrational relaxation coupled with solvent collisional deactivation due to an exergonic ESIPT reaction. The short viscosity-sensitive population decay is intriguing. Since the population decay and the steady-state emission yield are independent of the O–D substitution, the quenching process associated with high-frequency O–H vibration motions can be discarded. Instead, the dominant quenching process has been concluded to originate from one-bond (the exo C(5)–C(4)–C(3) bond) flip cis–trans isomerization diabatically from the excited-state cis tautomer to the ground-state trans tautomer. A comprehensive discussion of the viscosity-dependent lifetimes has been elaborated in our recent report.[11] This viewpoint is also supported qualitatively by the increase in the population lifetimes upon increasing the solvent viscosity for other title complexes (see Table 1). It is also noteworthy that the decay dynamics of **1b** in polar solvents is very complicated, involving multiple decay components. Due to the $-OCH_3$ electron donating group, the hydrogen-bonding strength of **1b** is substantially weaker than those of the other derivatives (vide supra). The weak hydrogen bonding strength, on the one hand, indicates the possible *E*/*Z* equilibrium in the ground state for **1b** in solution. On the other hand, for such a weak hydrogen bonding system, excited-state deprotonation to the surrounding solvent rather than intramolecular proton transfer may take place in a polar medium, forming the anionic species. Overlapping among *E*, *Z*, and anionic forms seriously complicates the results and analyses. The relevant discussion is complicated and deviates from the core issue of this study. Thus, only the lifetime of **1b** in cyclohexane is reported in Table 1.

The population decay time in cyclohexane correlates well with the weak to moderate steady-state tautomer emission, for which the quantum yield ranges from $(8.1 \pm 2) \times 10^{-5}$ for **1a** to $(2.0 \pm 0.2) \times 10^{-1}$ for **1g**. As observed in several derivatives of the core chromophore of GFP, *p*-HBDI, the population decay is even faster, which has been correlated with an efficient quenching process invoking similar cis–trans isomerization mechanisms.[7] However, in comparison to the Φ_f value of $<10^{-4}$ for *p*-HBDI, the substantially higher tautomer emission yield for the title compounds, except for **1a**, may be attributed to intramolecular hydrogen bond formation, which in part hinders the exocyclic torsional deformation such that the radiationless deactivation is reduced. The rather low yield of $(8.1 \pm 2) \times 10^{-5}$ for **1a** in cyclohexane may be rationalized by its longest wavelength tautomer emission at 670 nm, such that any additional quenching is possible due to the rather low energy gap; for example, the energy gap law, i.e. the quenching of emission by high-frequency vibration overtones and/or low-frequency motions associated with hydrogen bonds, may be operative.[13]

The quenching mechanism invoking rotation around the exo-C(5)–C(4)–C(3) bond incorporates large-amplitude motion and should be greatly inhibited in rigid media. Support of this viewpoint is given by the intense tautomer emission observed in the solid state for **1a**–**g**. As shown in Figure 5 and Table 2, depending on the electronic properties and position of the substituent, a wide range of tautomer emission can be tuned from 670 nm (**1a**) to 560 nm (**1g**) with a quantum yield as high as 0.1–0.9 in the solid film. The naked-eye view of the

dx.doi.org/10.1021/jo2012384 | J. Org. Chem. 2011, 76, 8189–8202

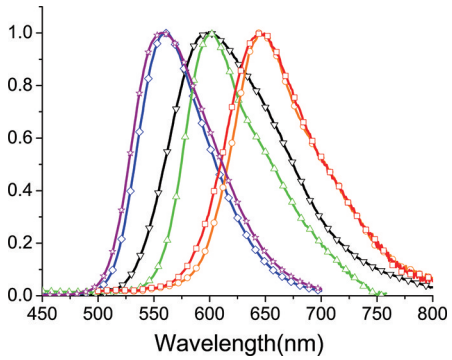

Figure 5. Solid-state emission spectra of **1a** (red □), **1b** (orange ○), **1c** (green △), **1d** (black ▽), **1e** (blue ◇), and **1f** (purple ☆).

Table 2. Photophysical Properties of 1a–g Recorded in the Solid State[a]

compd	substituent	λ_{em} (nm)	Φ_F	τ_{obsd} (ns)	τ_r (ns)
1a	–Ph	649	0.09	0.5	5.9
1b	–OMe	643	0.19	0.7	3.7
1c	–Br	605	0.59	3.5	5.9
1d	–H	595	0.4	1.7	4.3
1e	–CN	570	0.84	6	7.1
1f	$-CF_3$	560	0.85	6.3	7.4
1g	$-NO_2$	560	0.9	9.2	10.2

[a] τ_r stands for the radiative decay time and is calculated by $\tau_r = \tau_{obsd}/\Phi_F$, in which τ_{obsd} is the observed decay time and Φ_F denotes the emission yield.

emission color for **1b,d,f** in the solid state is also demonstrated in the abstract and table of contents artwork. The high emission yield also correlates well with the rather long population decay time of subnanoseconds to nanoseconds for **1a–g** in the solid state (see Table 2).

2.5. Computation and Electrochemistry. Supplementary support of the above structural and photophysical properties and their relationship are further provided by a computational approach. Theoretical confirmation of the underlying basis for the photophysical properties of **1a–g** and their tautomerized isomers are provided by Hartree–Fock calculations (see the Experimental Section). The optimized geometries of **1a–g** all demonstrated the existence of a seven-membered-ring intramolecular hydrogen bond between –OH and the N(2) atom (vide supra). On the basis of the TDB3LYP/6-31++G(d′,p′) method, the $S_0 \rightarrow S_1$ transition of **1a–g** can be mainly attributed to a HOMO → LUMO transition, for which HOMOs and LUMOs for the representative **1b**, **1d**, **1e**, and **1f** are drawn to exemplify the electron donor OCH_3, –H, and electron acceptors CN and CF_3 as the substituents, respectively, at the R_1 position (see Scheme 2A). Furthermore, the Franck–Condon type of emission can also be calculated on the basis of the TDB3LYP/HF method. Accordingly, HOMOs and LUMOs contributing to the $S_0' \rightarrow S_1'$ (the prime denotes the proton-transfer tautomer species) transition of the tautomer also can be calculated for **1a–g**, among which the representative **1d** is depicted in the last row of Figure 6.

In agreement with the aforementioned absorption spectroscopy, both $S_0 \rightarrow S_1$ and $S_0' \rightarrow S_1'$ types of transitions can be clearly ascribed to a $\pi \rightarrow \pi^*$ transition. For both transitions, the electron density was mainly located in the phenol fragment in the HOMO, while it is largely located at the imidazolone

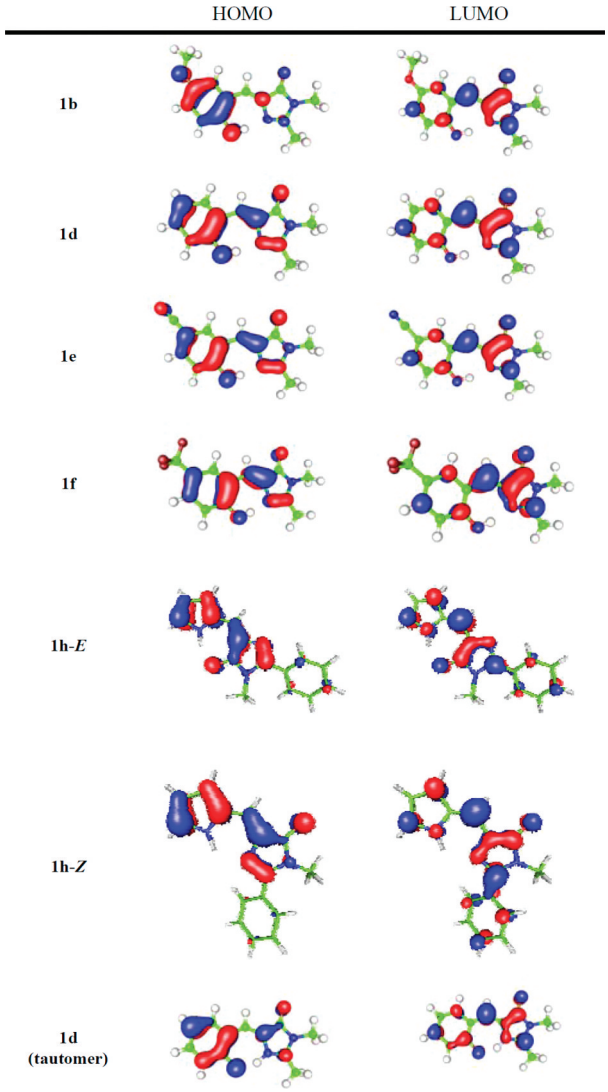

Figure 6. HOMOs and LUMOs involved in the $S_0 \rightarrow S_1$ transition for **1b,d–f** and the tautomer of **1d**.

moiety for the LUMO. Intuitively, adding an electron-donating group at the benzene (imidazolone) moiety causes an increase of energy in the HOMO (LUMO), hence the decrease (increase) of the lowest lying transition. Vice versa, adding an electron-withdrawing substituent should cause the inverse effect.

The above viewpoint is also supported experimentally by electrochemical measurements, in which the oxidation potential (HOMO) of **1a–g** was measured by cyclic voltammetry (CV) with ferrocene as the reference. The LUMO energy level of **1f** was then calculated by adding the lowest energy UV–vis absorption gap onto the HOMO level. As given in Table 3, it is evident that substituents with electron-donating nature at the C(9) position, such as $-OCH_3$ in **1b**, give a HOMO value of −5.55 eV, which is higher than that (−5.75 eV) of **1d**. For **1g** possessing a strong $-NO_2$ electron-withdrawing nature at the C(9) position, the HOMO value of −6.15 eV is the lowest among **1a–g**. Conversely, in comparison to the LUMO of −3.00 eV in nonsubstituted **1d**, adding a phenyl group at the C(1) position in **1a** decreases the LUMO energy to −3.32 eV simply due to the elongation of the resonance effect in LUMO. The results firmly support the original synthetic strategy aimed

dx.doi.org/10.1021/jo2012384 | J. Org. Chem. 2011, 76, 8189–8202

Table 3. Electrochemical Properties of 1a−g[a]

compd	E_{ox} (V vs Ag/AgCl)[b]	HOMO (eV)[c]	LUMO (eV)[c]	energy gap (eV)[d]
1a	1.47	−5.85	−3.32	2.53
1b	1.17	−5.55	−3.11	2.44
1c	1.3S	−5.76	−3.15	2.61
1d	1.37	−5.75	−3.00	2.75
1e	1.52	−5.90	−3.05	2.85
1f	1.53	−5.91	−3.01	2.90
1g	1.77	−6.15	−3.00	3.15

[a]Values obtained with 1.0 × 10 M solutions of **1a−g** in acetonitrile using 0.10 M tetrabutylanmonium pcrchlorate (TBAP) as supporting electrolyte. [b]The $Ag/AgNO_3$ reference electrode was calibrated using Fc/Fc^+. [c]The energy levels of the LUMO were calculated using the equations E_{HOMO} (eV) = −4.88 − (E_{ox} − E_{Fc/Fc^+}) and E_{LUMO} (eV) = E_{HOMO} + E_g. [d]The energy gap (E_g) is calculated from the absorption onset of each compound.

at fine-tuning the HOMO and LUMO energetics and hence the luminescence energy gap.

Figure 6 also depicts the HOMO and LUMO for both **1h-*E*** and **1h-*Z***. Upon careful examination, one can note that upon replacing the phenol by the pyrrolic moiety, forming either **1h-*E*** or **1h-*Z***, the electron density of HOMO in **1h** is mainly located at the π-conjugated system spreading from the pyrrolic to the immidazole moieties, whereas the pyrrolic N atom is not involved. This may result in a negligible increase of acidity of the pyrrolic proton upon excitation, rationalizing the prohibition of ESIPT for both **1h-*E*** and **1h-*Z*** forms (vide supra).

We then simply utilize the (lowest) absorption and emission peak frequencies as the first excitation energy gap for normal and proton-transfer tautomer, respectively. These values are added to the calculated relative energy between normal and tautomer species in the ground state. The results indicate that ESIPT for **1a−g** is a thermodynamically favorable process. For example, as depicted in Figure S55 (see the Supporting Information), ESIPT is estimated to be 8.82 kcal/mol thermally favorable for the case of **1d**. Moreover, upon Franck−Condon excitation and execution of the geometry relaxation (see the Experimental Section), the TDDFT method could not locate the energy minimum of the excited normal species, the result of which is consistent with a barrierless, perhaps coherent type of ESIPT process concluded experimentally using **1d**.[11]

2.6. Fabrication of OLEDs. To test the applicability of the titled *o*-hydroxy GFP chromophores as emitters in electroluminescence (EL),[14] we then selected **1d** as the dopant with the structures of ITO/PEDOT:PSS (30 nm)/NPB (20 nm)/TCTA (5 nm)/CBP:**1d** (5 wt %, 25 nm)/TPBI (50 nm)/LiF (0.5 nm)/Al (100 nm). We used 4,4′-*N*,*N*-dicarbazolyl-1,1′-biphenyl (CBP) as a host that possesses suitable energy levels (HOMO/LUMO = −5.9/−2.6 eV) to confine excitons within the guest emitter.[15] Here, the conducting polymer poly(ethylene dioxythiophene)/poly(styrene sulfonate) (PEDOT:PSS) was used as the hole-injection layer, 4,4′-bis[*N*-(1-naphthyl)-*N*-phenylamino]biphenyl (NPB) and 4,4′,4″-tri(*N*-carbazolyl)triphenylamine (TCTA) were used as hole-transport layers, 1,3,5-tris(*N*-phenylbenzimidizol-2-yl)benzene (TPBI) was used as an electron-transport and hole-blocking layer, LiF was used as an electron-injection layer, and Al was used as a cathode, respectively. The device configuration is depicted in Figure S56 of the Supporting Information. Consequently, an orange EL spectrum from **1d** was obtained (the inset of Figure 7), which corresponds well to the thin film PL spectrum shown in Figure 2. In our preliminary test, the device revealed a maximum brightness of 5790 cd m^{-2} at 17.5 V (1610 mA cm^{-2}) with the CIE coordinates of (0.55, 0.43). As Figure 7

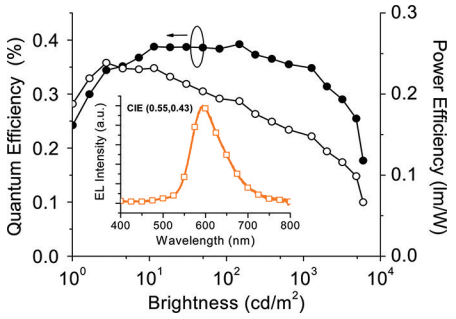

Figure 7. External quantum (η_{ext}) and power efficiencies (η_p) as a function of brightness. Inset: EL spectrum of the device.

shows, the maximum external quantum efficiency (η_{ext}) and power efficiency (η_p) were 0.40% (0.82 cd A^{-1}) and 0.24 lm W^{-1}, respectively (also see Table S1 in the Supporting Information). We believe that the efficiency of this *o*-hydroxy-GFP device can be further improved by optimizing device configurations. Work regarding full optimization of devices fabricated with **1a−g** is in progress.

3. CONCLUSION

In summary, we have reported the synthesis, characterization, and corresponding electrochemical and photophysical properties of a series of *o*-hydroxy analogues, compounds **1a−g**, of the green fluorescent protein chromophore. All title compounds possess a *Z* conformation and undergo a remarkable ESIPT reaction via a pre-existing seven-membered-ring hydrogen bond. In comparison to the natural *p*-hydroxy-GFP core chromophore, i.e. *p*-HBDI, the intramolecular hydrogen bond in **1a−g** plays a key role in suppressing the nonradiative deactivation pathway associated with cis (*Z* form)−trans (*E* form) isomerization.[11] Depending on the electron donating/withdrawing or resonance properties of the substituents, the proton transfer emission can be fine-tuned from 560 nm (**1g**) to 670 nm (**1a**). Although the tautomer emission yield is weak to moderate in solution, due to the lack of rotation at the exo C−C bond, the quantum yield is as high as 0.1−0.9 for the title compounds in the solid state. Fabrication of OLEDs using **1d** as a prototype has been successfully carried out, demonstrating its latent potential in recently popular proton-transfer types of lighting sources.[16] Synthetic approaches with other relevant analogues are feasible, as supported by another series of pyrrolic analogues **1h** (see Scheme 2). Also, one can envisage that further substitution at the R_2 site (see Scheme 2A) by e.g. imidazole may lead to the derivation of a series of *o*-hydroxy red fluorescent protein (RFP) core chromophores (the Kaede dye).[1a−d] We also anticipate that the radiationless quenching process may be further reduced by anchoring bulky groups at the C(4) position (see Scheme 1), generating a series of isomers of *p*-HBDI with remarkable ESIPT properties and intense proton-transfer tautomer emission suitable for lighting applications.

dx.doi.org/10.1021/jo2012384 | J. Org. Chem. 2011, 76, 8189−8202

4. EXPERIMENTAL SECTION

4.1. Synthesis. The synthetic route of **1d** (*o*-HBDI) has been described in our previous report and is thus omitted from the following synthetic elaboration.[10]

4.2. Physical and Spectroscopic Characterization Data for Compounds 1a–g, 1h-*Z*, and 1h-*E*. *4.2.1. (Z)-4-(2-Methoxybenzylidene)-2-phenyloxazol-5(4H)-one (**3a**).* Hippuric acid (5.0 g, 27.9 mmol), sodium acetate (2.3 g, 28.0 mmol), *o*-anisaldehyde (3.8 g, 27.9 mmol), and acetic anhydride (50 mL) were heated at 80 °C with stirring for 4 h. After the solvent was removed, the crude product was purified by silica gel column chromatography with ethyl acetate/*n*-hexane (1/2) as eluent to afford **3a**: yellow solid; yield 5.5 g (71%); mp 110–111 °C; ^{1}H NMR (400 MHz, CD_2Cl_2, ppm) 8.89 (d, J = 8.8 Hz, 1H), 8.20–8.17 (m, 2H), 7.82 (s, 1H), 7.66 (t, J = 7.4 Hz, 1H), 7.58 (m, 2H), 7.48 (t, J = 8.6 Hz, 1H), 7.13 (t, J = 7.6 Hz, 1H), 6.99 (d, J = 8.4 Hz, 1H), 3.95 (s, 3H); ^{13}C NMR (100 MHz, CD_2Cl_2, ppm) 167.5, 163.1, 159.3, 133.1, 132.9, 132.7, 132.5, 128.9, 128.1, 125.8, 125.3, 122.5, 120.8, 110.8, 55.7; MS (EI, 70 eV) m/z (relative intensity) 279 (M^+, 100); HRMS calcd for $C_{17}H_{13}O_3N$ 279.0895, found 279.0891. Anal. Calcd for $C_{17}H_{13}O_3N$: C, 73.11; H, 4.69; N, 5.02. Found: C, 73.37; H, 4.75; N, 5.22.

*4.2.2. (Z)-4-(2-Methoxybenzylidene)-1-methyl-2-phenyl-1H-imidazol-5(4H)-one (**2a**).* (*Z*)-4-(2-Methoxybenzylidene)-2-phenyloxazol-5(4*H*)-one (**3a**; 1.0 g, 3.6 mmol) was added to potassium carbonate (0.5 g, 3.6 mmol) in a 50 mL round-bottom flask, in which 20 mL of ethanol (95%) and 1.0 mL of methylamine (40% aqueous) were then added. The reaction mixture was refluxed for 4 h. After cooling, the mixture was neutralized with 10% HCl and extracted with CH_2Cl_2 (3 × 25 mL). After solvent was removed, the crude product was purified by silica gel column chromatography with ethyl acetate/*n*-hexane (1/2) as eluent to afford **2a**: yellow solid; yield 0.7 g (67%); mp 126–127 °C; ^{1}H NMR (400 MHz, $CDCl_3$, ppm) 8.92 (d, J = 7.6 Hz, 1H), 7.85–7.83 (m, 3H), 7.56–7.52 (m, 3H), 7.37 (t, J = 8.4 Hz, 1H), 7.04 (t, J = 7.6 Hz, 1H), 6.91 (d, J = 8.3 Hz, 1H), 3.90 (s, 3H), 3.37 (s, 3H); ^{13}C NMR (100 MHz, $CDCl_3$, ppm) 171.7, 161.8, 159.3, 138.4, 133.3, 131.9, 131.3, 129.5, 128.7, 128.6, 123.4, 122.9, 120.9, 110.5, 55.5, 29.0; MS (EI, 70 eV) m/z (relative intensity) 292 (M^+, 100); HRMS calcd for $C_{18}H_{16}O_2N_2$ 292.1212, found 292.1219. Anal. Calcd for $C_{18}H_{16}O_2N_2$: C, 73.95; H, 5.52; N, 9.58. Found: C, 73.69; H, 5.56; N, 9.80.

*4.2.3. (Z)-4-(2-Hydroxybenzylidene)-1-methyl-2-phenyl-1H-imidazol-5(4H)-one (**1a**).* (*Z*)-4-(2-Methoxybenzylidene)-1-methyl-2-phenyl-1*H*-imidazol-5(4*H*)-one (**2a**; 300 mg, 1.0 mmol) was dissolved in 10 mL of dichloromethane in a 50 mL round-bottom flask, and the flask was placed in an ice bath at 0 °C. A solution of boron tribromide (4.0 mL, 1.0 M solution in dichloromethane) was added carefully to the stirred solution under a nitrogen atmosphere. After 4 h, the reaction mixture was cooled and then hydrolyzed by careful shaking with 10 mL of water and extracted twice with 10 mL of dichloromethane. The combined organic phases were then dried over magnesium sulfate, filtered, and evaporated in vacuo, and the crude product was purified by silica gel column chromatography with ethyl acetate/*n*-hexane (1/2) as eluent to afford **1a**: yellow solid; yield 265 mg (94%); mp 150–151 °C; ^{1}H NMR (400 MHz, CD_2Cl_2, ppm) 13.94 (s, 1H), 7.84–7.81 (m, 2H), 7.66–7.57 (m, 3H), 7.38–7.35 (m, 2H), 7.28 (s, 1H), 6.94 (d, J = 8.5 Hz, 1H), 6.88 (t, J = 7.4 Hz, 1H), 3.39 (s, 3H); ^{13}C NMR (100 MHz, CD_2Cl_2, ppm) 168.5, 158.7, 157.6, 136.4, 134.2, 133.3, 132.0, 130.7, 129.0, 128.3, 127.8, 119.9, 119.3, 119.0, 29.1; MS (EI, 70 eV) m/z (relative intensity) 278 (M^+, 100); HRMS calcd for $C_{17}H_{14}O_2N_2$ 278.1055, found 278.1049. Anal. Calcd for $C_{17}H_{14}O_2N_2$: C, 73.37; H, 5.07; N, 10.07. Found: C, 73.21; H, 5.11; N, 10.29. Yellow needle-shaped crystals suitable for the crystallographic studies reported here were isolated over a period of 6 weeks by slow evaporation from the chloroform solution.

*4.2.4. (Z)-4-(2,5-Dimethoxybenzylidene)-2-methyloxazol-5(4H)-one (**3b**).* *N*-Acetylglycine (2.0 g, 17.1 mmol), sodium acetate (1.4 g, 17.1 mmol), 2,5-dimethoxybenzaldehyde (2.8 g, 16.8 mmol), and acetic anhydride (40 mL) were heated at 80 °C with stirring for 4 h. After solvent was removed, the crude product was purified by silica gel column chromatography with ethyl acetate/*n*-hexane (1/2) as eluent to afford **3b**: yellow solid; yield 3.2 g (76%); mp 104–105 °C; ^{1}H NMR (400 MHz, $CDCl_3$, ppm) 8.26 (d, J = 2.4 Hz, 1H), 7.67 (s, 1H), 6.93 (dd, J_1 = 8.8 Hz, J_2 = 2.4 Hz, 1H), 6.81 (d, J = 8.8 Hz, 1H), 3.83 (s, 3H), 3.80 (s, 3H), 2.36 (s, 3H); ^{13}C NMR (100 MHz, $CDCl_3$, ppm) 167.9, 165.4, 153.9, 153.4, 131.9, 125.3, 122.6, 119.2, 116.5, 111.9, 56.1, 55.8, 15.6; MS (EI, 70 eV) m/z (relative intensity) 247 (M^+, 100); HRMS calcd for $C_{13}H_{13}O_4N$ 247.0845, found 247.0841. Anal. Calcd for $C_{13}H_{13}O_4N$: C, 63.15; H, 5.30; N, 5.67. Found: C, 63.01; H, 5.36; N, 5.81.

*4.2.5. (Z)-4-(2,5-Dimethoxybenzylidene)-1,2-dimethyl-1H-imidazol-5(4H)-one (**2b**).* (*Z*)-4-(2,5-Dimethoxybenzylidene)-2-methyloxazol-5(4*H*)-one (**3b**; 1.2 g, 4.8 mmol) was added to potassium carbonate (0.7 g, 5.1 mmol) in a 50 mL round-bottom flask, in which 15 mL of ethanol (95%) and 1.0 mL of methylamine (40% aqueous) were then added. The reaction mixture was refluxed for 4 h. After cooling, the mixture was neutralized with 10% HCl and extracted with CH_2Cl_2 (3 × 25 mL). After solvent was removed, the crude product was purified by silica gel column chromatography with ethyl acetate/*n*-hexane (1/1) as eluent to afford **2b**: yellow solid; yield 0.81 g (65%); mp 118–119 °C; ^{1}H NMR (400 MHz, $CDCl_3$, ppm) 8.39 (d, J = 3.0 Hz, 1H), 7.58 (s, 1H), 6.87 (dd, J_1 = 9.0 Hz, J_2 = 3.0 Hz, 1H), 6.78 (d, J = 9.1 Hz, 1H), 3.79 (s, 3H), 3.77 (s, 3H), 3.12 (s, 3H), 2.29 (s, 3H); ^{13}C NMR (100 MHz, $CDCl_3$, ppm) 170.6, 161.9, 153.8, 153.4, 138.3, 123.6, 120.8, 117.8, 117.0, 111.7, 56.1, 55.7, 26.4, 15.6; MS (EI, 70 eV) m/z (relative intensity) 260 (M^+, 54), 229 (100); HRMS calcd for $C_{14}H_{16}O_3N_2$ 260.1161, found 260.1156. Anal. Calcd for $C_{14}H_{16}O_3N_2$: C, 64.60; H, 6.20; N, 10.76. Found: C, 64.42; H, 6.26; N, 10.92.

*4.2.6. (Z)-4-(2-Hydroxy-5-methoxybenzylidene)-1,2-dimethyl-1H-imidazol-5(4H)-one (**1b**).* (*Z*)-4-(2,5-Dimethoxybenzylidene)-1,2-dimethyl-1*H*-imidazol-5(4*H*)-one (**2b**; 286 mg, 1.1 mmol) was dissolved in 10 mL of dichloromethane in a 50 mL round-bottom flask, and the flask was placed in an ice bath at 0 °C. A solution of boron tribromide (4.4 mL, 1.0 M solution in dichloromethane) was added carefully to the stirred solution under a nitrogen atmosphere. After 4 h, the reaction mixture was cooled and then hydrolyzed by careful shaking with 10 mL of water and extracted twice with 10 mL of dichloromethane. The combined organic phases were then dried over magnesium sulfate, filtered, and evaporated in vacuo, and the crude product was purified by silica gel column chromatography with ethyl acetate/*n*-hexane (1/1) as eluent to afford **1b**: yellow solid; yield 241 mg (89%); mp 146–147 °C; ^{1}H NMR (400 MHz, CD_2Cl_2, ppm) 13.26 (s, 1H), 7.09 (s, 1H), 6.97 (dd, J_1 = 8.9 Hz, J_2 = 3.0 Hz, 1H), 6.88 (d, J = 8.9 Hz, 1H), 6.76 (d, J = 3.0 Hz, 1H), 3.76 (s, 3H), 3.20 (s, 3H), 2.36 (s, 3H); ^{13}C NMR (100 MHz, CD_2Cl_2, ppm) 167.9, 157.7, 152.8, 152.2, 133.2, 129.8, 121.7, 120.0, 119.4, 118.3, 55.7, 26.7, 15.1; MS (EI, 70 eV) m/z (relative intensity) 246 (M^+, 100); HRMS calcd for $C_{13}H_{14}O_3N_2$ 246.1004, found 246.1008. Anal. Calcd for $C_{13}H_{14}O_3N_2$: C, 63.40; H, 5.73; N, 11.38. Found: C, 63.26; H, 5.77; N, 11.56. Yellow needle-shaped crystals suitable for the crystallographic studies reported here were isolated over a period of 5 weeks by slow evaporation from the chloroform solution.

*4.2.7. (Z)-4-(5-Bromo-2-methoxybenzylidene)-2-methyloxazol-5(4H)-one (**3c**).* *N*-Acetylglycine (2.0 g, 17.1 mmol), sodium acetate (1.4 g, 17.1 mmol), 5-bromo-2-methoxybenzaldehyde (3.6 g, 16.7 mmol), and acetic anhydride (40 mL) were heated at 80 °C with stirring for 4 h. After solvent was removed, the crude product was purified by silica gel column chromatography with ethyl acetate/*n*-hexane (1/2) as eluent to afford **3c**: yellow solid; yield 3.6 g (71%); mp 145–146 °C; ^{1}H NMR (400 MHz, $CDCl_3$, ppm) 8.75 (d, J = 1.7 Hz, 1H), 7.57 (s, 1H), 7.46 (dd, J_1 = 8.4 Hz, J_2 = 1.7 Hz, 1H), 6.78 (d, J = 8.8 Hz, 1H), 3.86 (s, 3H), 2.39 (s, 3H); ^{13}C NMR (100 MHz, $CDCl_3$, ppm) 167.6, 166.3, 158.0, 135.0, 134.7, 132.7, 124.0, 123.5, 113.3, 112.4, 55.9, 15.6; MS (EI, 70 eV) m/z (relative intensity) 295 (M^+, 70), 225 (100); HRMS calcd for $C_{12}H_{10}BrO_3N$ 294.9844, found 294.9848. Anal. Calcd for $C_{12}H_{10}O_3NBr$: C, 48.67; H, 3.40; N, 4.73. Found: C, 48.49; H, 3.42; N, 4.87.

*4.2.8. (Z)-4-(5-Bromo-2-methoxybenzylidene)-1,2-dimethyl-1H-imidazol-5(4H)-one (**2c**).* (*Z*)-4-(5-Bromo-2-methoxybenzylidene)-2-methyloxazol-5(4*H*)-one (**3c**; 1.3 g, 4.4 mmol) was added to potassium carbonate (0.7 g, 5.1 mmol) in a 50 mL round-bottom

flask, in which 15 mL of ethanol (95%) and 1.0 mL of methylamine (40% aqueous) were then added. The reaction mixture was refluxed for 4 h. After cooling, the mixture was neutralized with 10% HCl and extracted with CH_2Cl_2 (3 × 25 mL). After solvent was removed, the crude product was purified by silica gel column chromatography with ethyl acetate/*n*-hexane (1/1) as eluent to afford **2c**: yellow solid; yield 0.88 g (68%); mp 157−158 °C; ^{1}H NMR (400 MHz, $CDCl_3$, ppm) 8.88 (d, J = 2.7 Hz, 1H), 7.52 (s, 1H), 7.42 (dd, J_1 = 8.8 Hz, J_2 = 2.4 Hz, 1H), 6.76 (d, J = 8.8 Hz, 1H), 3.86 (s, 3H), 3.17 (s, 3H), 2.37 (s, 3H); ^{13}C NMR (100 MHz, $CDCl_3$, ppm) 170.5, 162.8, 157.9, 138.9, 135.0, 133.8, 125.0, 119.49, 113.2, 112.2, 55.8, 26.5, 15.6; MS (EI, 70 eV) m/z (relative intensity) 308 (M^+, 92), 279 (100); HRMS calcd for $C_{13}H_{13}BrO_2N_2$ 308.0160, found 308.0168. Anal. Calcd for $C_{13}H_{13}O_2N_2Br$: C, 50.50; H, 4.24; N, 9.06. Found: C, 50.28; H, 4.40; N, 9.28.

*4.2.9. (Z)-4-(5-Bromo-2-hydroxybenzylidene)-1,2-dimethyl-1H-imidazol-5(4H)-one (**1c**).* (*Z*)-4-(5-Bromo-2-methoxybenzylidene)-1,2-dimethyl-1*H*-imidazol-5(4*H*)-one (**2c**; 340 mg, 1.1 mmol) was dissolved in 10 mL of dichloromethane in a 50 mL round-bottom flask, and the flask was placed in an ice bath at 0 °C. A solution of boron tribromide (4.4 mL, 1.0 M solution in dichloromethane) was added carefully to the stirred solution under a nitrogen atmosphere. After 4 h, the reaction mixture was cooled and then hydrolyzed by careful shaking with 10 mL of water and extracted twice with 10 mL of dichloromethane. The combined organic phases were then dried over magnesium sulfate, filtered, and evaporated in vacuo, and the crude product was purified by silica gel column chromatography with ethyl acetate/*n*-hexane (1/1) as eluent to afford **1c**: yellow solid; yield 300 mg (92%); mp 172−173 °C; ^{1}H NMR (400 MHz, CD_2Cl_2, ppm) 13.82 (s, 1H), 7.39 (d, J = 9.3 Hz, 1H), 7.36 (s, 1H), 7.03 (s, 1H), 6.84 (d, J = 9.3 Hz, 1H), 3.23 (s, 3H), 2.40 (s, 3H); ^{13}C NMR (100 MHz, CD_2Cl_2, ppm) 167.6, 158.4, 157.6, 137.6, 136.3, 133.5, 128.3, 121.4, 121.1, 110.8, 26.8, 15.2; MS (EI, 70 eV) m/z (relative intensity) 294 (M^+, 100); HRMS calcd for $C_{12}H_{11}BrO_2N_2$ 294.0004, found 294.0003. Anal. Calcd for $C_{12}H_{11}O_2N_2Br$: C, 48.84; H, 3.76; N, 9.49. Found: C, 48.66; H, 3.80; N, 9.61. Yellow needle-shaped crystals suitable for the crystallographic studies reported here were isolated over a period of 4 weeks by slow evaporation from the chloroform solution.

*4.2.10. (Z)-4-Methoxy-3-((2-methyl-5-oxooxazol-4(5H)-ylidene)-methyl)benzonitrile (**3e**).* *N*-Acetylglycine (2.0 g, 17.1 mmol), sodium acetate (1.4 g, 17.1 mmol), 3-formyl-4-methoxybenzonitrile (2.7 g, 17.4 mmol), and acetic anhydride (40 mL) were heated at 80 °C with stirring for 4 h. After solvent was removed, the crude product was purified by silica gel column chromatography with ethyl acetate/*n*-hexane (1/2) as eluent to afford **3e**: yellow solid; yield 3.1 g (77%); mp 151−152 °C; ^{1}H NMR (400 MHz, $CDCl_3$, ppm) 8.98 (s, 1H), 7.65 (d, J = 8.5 Hz, 1H), 7.55 (s, 1H), 6.97 (d, J = 8.8 Hz, 1H), 3.95 (s, 3H), 2.41 (s, 3H); ^{13}C NMR (100 MHz, $CDCl_3$, ppm) 167.2, 161.4, 136.6, 135.8, 133.7, 123.2, 122.2, 118.7, 111.4, 104.6, 56.1, 15.7. (one carbon nuclei could not be observed or resolved); MS (EI, 70 eV) m/z (relative intensity) 242 (M^+, 100); HRMS calcd for $C_{13}H_{10}O_3N_2$ 242.0691, found 242.0693. Anal. Calcd for $C_{13}H_{10}O_3N_2$: C, 64.46; H, 4.16; N, 11.56. Found: C, 64.34; H, 4.22; N, 11.68.

*4.2.11. (Z)-3-((1,2-Dimethyl-5-oxo-1H-imidazol-4(5H)-ylidene)-methyl)-4-methoxybenzonitrile (**2e**).* (*Z*)-4-Methoxy-3-((2-methyl-5-oxooxazol-4(5*H*)-ylidene)methyl)benzonitrile (**3e**; 1.1 g, 4.5 mmol) was added to potassium carbonate (0.7 g, 5.1 mmol) in a 50 mL round-bottom flask, in which 15 mL of ethanol (95%) and 1.0 mL of methylamine (40% aqueous) were then added. The reaction mixture was refluxed for 4 h. After cooling, the mixture was neutralized with 10% HCl and extracted with CH_2Cl_2 (3 × 25 mL). After solvent was removed, the crude product was purified by silica gel column chromatography with ethyl acetate/*n*-hexane (1/1) as eluent to afford **2e**: yellow solid; yield 0.69 g (60%); mp 162−163 °C; ^{1}H NMR (400 MHz, $CDCl_3$, ppm) 9.11 (s, 1H), 7.61 (d, J = 8.8 Hz, 1H), 7.48 (s, 1H), 6.95 (d, J = 8.8 Hz, 1H), 3.95 (s, 3H), 3.19 (s, 3H), 2.39 (s, 3H); ^{13}C NMR (100 MHz, $CDCl_3$, ppm) 170.3, 163.8, 161.4, 139.8, 136.9, 134.8, 124.2, 119.1, 118.0, 111.1, 104.4, 55.9, 26.6, 15.6; MS (EI, 70 eV) m/z (relative intensity) 255 (M^+, 100); HRMS calcd for $C_{14}H_{13}O_2N_3$ 255.1008, found 255.1010. Anal. Calcd for $C_{14}H_{13}O_2N_3$: C, 65.87; H, 5.13; N, 16.46. Found: C, 65.65; H, 5.19; N, 16.66.

*4.2.12. (Z)-3-((1,2-Dimethyl-5-oxo-1H-imidazol-4(5H)-ylidene)-methyl)-4-hydroxybenzonitrile (**1e**).* (*Z*)-3-((1,2-Dimethyl-5-oxo-1*H*-imidazol-4(5*H*)-ylidene)methyl)-4-methoxybenzonitrile (**2e**; 280 mg, 1.1 mmol) was dissolved in 10 mL of dichloromethane in a 50 mL round-bottom flask, and the flask was placed in an ice bath at 0 °C. A solution of boron tribromide (4.4 mL, 1.0 M solution in dichloromethane) was added carefully to the stirred solution under a nitrogen atmosphere. After 4 h, the reaction mixture was cooled and then hydrolyzed by careful shaking with 10 mL of water and extracted twice with 10 mL of dichloromethane. The combined organic phases were then dried over magnesium sulfate, filtered, and evaporated in vacuo, and the crude product was purified by silica gel column chromatography with ethyl acetate/*n*-hexane (1/1) as eluent to afford **1e**: yellow solid; yield 250 mg (95%); mp 186−187 °C; ^{1}H NMR (400 MHz, CD_2Cl_2, ppm) 14.70 (s, 1H), 7.62 (s, 1H), 7.55 (d, J = 8.4 Hz, 1H), 6.99 (s, 1H), 6.95 (d, J = 8.5 Hz, 1H), 3.20 (s, 3H), 2.40 (s, 3H); ^{13}C NMR (100 MHz, CD_2Cl_2, ppm) 167.2, 162.0, 160.1, 140.3, 136.1, 134.2, 126.3, 120.6, 120.4, 118.6, 102.6, 26.7, 15.1; MS (EI, 70 eV) m/z (relative intensity) 241 (M^+, 100); HRMS calcd for $C_{13}H_{11}O_2N_3$ 241.0851, found 241.0847. Anal. Calcd for $C_{13}H_{11}O_2N_3$: C, 64.72; H, 4.60; N, 17.42. Found: C, 64.60; H, 4.64; N, 17.60. Yellow needle-shaped crystals suitable for the crystallographic studies reported here were isolated over a period of 5 weeks by slow evaporation from the chloroform solution.

*4.2.13. (Z)-4-(2-Methoxy-5-(trifluoromethyl)benzylidene)-2-methyl-4H-oxazol-5-one (**3f**).* *N*-Acetylglycine (2.0 g, 17.1 mmol), sodium acetate (1.4 g, 17.1 mmol), 2-methoxy-5-(trifluoromethyl)-benzaldehyde (3.5 g, 17.1 mmol), and acetic anhydride (40 mL) were heated at 80 °C with stirring for 4 h. After solvent was removed, the crude product was purified by silica gel column chromatography with ethyl acetate/*n*-hexane (1/2) as eluent to afford **3f**: yellow solid; yield 4.0 g (82%); mp 161−162 °C; ^{1}H NMR (400 MHz, $CDCl_3$, ppm) 8.97 (s, 1H), 7.66 (s, 1H), 7.63 (d, J = 8.8 Hz, 1H), 6.98 (d, J = 8.8 Hz, 1H), 3.96 (s, 3H), 2.42 (s, 3H); ^{13}C NMR (100 MHz, $CDCl_3$, ppm) 167.2, 162.1, 136.1, 135.7, 133.8, 123.7, 122.5, 120.7, 116.7, 112.4, 111.4, 56.2, 15.6; MS (EI, 70 eV) m/z (relative intensity) 285 (M^+, 100); HRMS calcd for $C_{13}H_{10}F_3NO_3$ 285.0613, found 285.0616. Anal. Calcd for $C_{13}H_{10}O_3NF_3$: C, 54.74; H, 3.53; N, 4.91. Found: C, 54.52; H, 3.61; N, 5.05.

*4.2.14. (Z)-5-(2-Methoxy-5-(trifluoromethyl)benzylidene)-2,3-dimethyl-3,5-dihydroimidazol-4-one (**2f**).* (*Z*)-4-(2-Methoxy-5-(trifluoromethyl)benzylidene)-2-methyl-4*H*-oxazol-5-one (**3f**; 1.0 g, 3.5 mmol) was added to potassium carbonate (0.7 g, 5.1 mmol) in a 50 mL round-bottom flask, in which 15 mL of ethanol (95%) and 1.0 mL of methylamine (40% aqueous) were then added. The reaction mixture was refluxed for 4 h. After cooling, the mixture was neutralized with 10% HCl and extracted with CH_2Cl_2 (3 × 25 mL). After solvent was removed, the crude product was purified by silica gel column chromatography with ethyl acetate/*n*-hexane (1/1) as eluent to afford **2f**: yellow solid; yield 0.64 g (62%); mp 172−173 °C; ^{1}H NMR (400 MHz, $CDCl_3$, ppm) 9.08 (s, 1H), 7.58 (s, 1H), 7.56 (d, J = 8.8 Hz, 1H), 6.96 (d, J = 8.8 Hz, 1H), 3.93 (s, 3H), 3.19 (s, 3H), 2.38 (s, 3H); ^{13}C NMR (100 MHz, $CDCl_3$, ppm) 170.3, 164.3, 138.8, 137.4, 134.7, 124.6, 121.4, 119.9, 116.2, 112.1, 111.3, 56.0, 26.9, 15.6; MS (EI, 70 eV) m/z (relative intensity) 298 (M^+, 100); HRMS calcd for $C_{14}H_{13}F_3N_2O_2$ 298.0929, found 298.0934. Anal. Calcd for $C_{14}H_{13}O_2N_2F_3$: C, 56.38; H, 4.39; N, 9.39. Found: C, 56.52; H, 4.45; N, 9.17.

*4.2.15. (Z)-5-(2-Hydroxy-5-(trifluoromethyl)benzylidene)-2,3-dimethyl-3,5-dihydroimidazol-4-one (**1f**).* (*Z*)-5-(2-Methoxy-5-(trifluoromethyl)benzylidene)-2,3-dimethyl-3,5-dihydro-imidazol-4-one (**2f**; 200 mg, 0.7 mmol) was dissolved in 10 mL of dichloromethane in a 50 mL round-bottom flask, and the flask was placed in an ice bath at 0 °C. A solution of boron tribromide (2.8 mL, 1.0 M solution in dichloromethane) was added carefully to the stirred solution under a nitrogen atmosphere. After 4 h, the reaction mixture was cooled and then hydrolyzed by careful shaking with 10 mL of water and extracted twice with 10 mL of dichloromethane. The

dx.doi.org/10.1021/jo2012384 | *J. Org. Chem.* 2011, 76, 8189−8202

combined organic phases were then dried over magnesium sulfate, filtered, and evaporated in vacuo, and the crude product was purified by silica gel column chromatography with ethyl acetate/*n*-hexane (1/1) as eluent to afford **1f**: yellow solid; yield 160 mg (84%); mp 190−191 °C; ^{1}H NMR (400 MHz, CD_2Cl_2, ppm) 14.18 (s, 1H), 7.68 (s, 1H), 7.56 (d, J = 8.4 Hz, 1H), 7.13 (s, 1H), 7.03 (d, J = 8.4 Hz, 1H), 3.25 (s, 3H), 2.51 (s, 3H); ^{13}C NMR (100 MHz, CD_2Cl_2, ppm) 167.1, 162.3, 138.4, 137.8, 135.9, 124.6, 121.3, 119.7, 116.0, 112.0, 111.1, 26.9, 15.6; MS (EI, 70 eV) m/z (relative intensity) 284 (M^+, 100); HRMS calcd for $C_{13}H_{11}F_3N_2O_2$ 284.0773, found 284.0776. Anal. Calcd for $C_{13}H_{11}O_2N_2F_3$: C, 54.93; H, 3.90; N, 9.86. Found: C, 54.75; H, 3.96; N, 9.98.

*4.2.16. (4Z)-4-(2-Methoxy-5-nitrobenzylidene)-2-methyloxazol-5(4H)-one (**3g**).* *N*-Acetylglycine (2.0 g, 17.1 mmol), sodium acetate (1.4 g, 17.1 mmol), 2-methoxy-5-nitrobenzaldehyde (3.1 g, 17.1 mmol), and acetic anhydride (40 mL) were heated at 80 °C with stirring for 4 h. After solvent was removed, the crude product was purified by silica gel column chromatography with ethyl acetate/*n*-hexane (1/2) as eluent to afford **3g**: yellow solid; yield 3.2 g (71%); mp 185−186 °C; ^{1}H NMR (400 MHz, $CDCl_3$, ppm) 9.52 (d, J = 2.6 Hz, 1H), 8.28 (dd, J_1 = 9.2 Hz, J_2 = 2.6 Hz, 1H), 7.56 (s, 1H), 6.99 (d, J = 9.2 Hz, 1H), 4.02 (s, 3H), 2.45 (s, 3H); ^{13}C NMR (100 MHz, $CDCl_3$, ppm) 167.5, 167.2, 162.9, 114.6, 134.1, 128.2, 127.6, 122.6, 122.3, 110.6, 56.6, 15.8; MS (EI, 70 eV) m/z (relative intensity) 262 (M^+, 100); HRMS calcd for $C_{12}H_{10}O_5N_2$ 262.0590, found 262.0596. Anal. Calcd for $C_{12}H_{10}O_5N_2$: C, 54.97; H, 3.84; N, 10.68. Found: C, 54.75; H, 3.92; N, 10.84.

*4.2.17. (4Z)-4-(2-Methoxy-5-nitrobenzylidene)-1,2-dimethyl-1H-imidazol-5(4H)-one (**2g**).* (4*Z*)-4-(2-Methoxy-5-nitrobenzylidene)-2-methyloxazol-5(4*H*)-one (**3g**; 1.2 g, 4.6 mmol) was added to potassium carbonate (0.7 g, 5.1 mmol) in a 50 mL round-bottom flask, in which 15 mL of ethanol (95%) and 1.0 mL of methylamine (40% aqueous) were then added. The reaction mixture was refluxed for 4 h. After cooling, the mixture was neutralized with 10% HCl and extracted with CH_2Cl_2 (3 × 25 mL). After solvent was removed, the crude product was purified by silica gel column chromatography with ethyl acetate/*n*-hexane (1/1) as eluent to afford **2g**: yellow solid; yield 0.79 g (62%); mp 197−198 °C; ^{1}H NMR (400 MHz, $CDCl_3$, ppm) 9.65 (d, J = 3.1 Hz, 1H), 8.22 (dd, J_1 = 8.9 Hz, J_2 = 3.1 Hz, 1H), 7.49 (s, 1H), 6.94 (d, J = 8.9 Hz, 1H), 3.98 (s, 3H), 3.18 (s, 3H), 2.40 (s, 3H); ^{13}C NMR (100 MHz, $CDCl_3$, ppm) 170.3, 164.1, 162.9, 141.5, 140.1, 128.5, 126.5, 123.7, 118.0, 110.3, 56.3, 26.6, 15.7; MS (EI, 70 eV) m/z (relative intensity) 275 (M^+, 100); HRMS calcd for $C_{13}H_{13}O_4N_3$ 275.0906, found 275.0902. Anal. Calcd for $C_{13}H_{13}O_4N_3$: C, 56.72; H, 4.76; N, 15.27. Found: C, 56.50; H, 4.80; N, 15.51.

*4.2.18. (4Z)-4-(2-Hydroxy-5-nitrobenzylidene)-1,2-dimethyl-1H-imidazol-5(4H)-one (**1g**).* (4*Z*)-4-(2-Methoxy-5-nitrobenzylidene)-1,2-dimethyl-1*H*-imidazol-5(4*H*)-one (**2g**; 300 mg, 1.1 mmol) was dissolved in 10 mL of dichloromethane in a 50 mL round-bottom flask, and the flask was placed in an ice bath at 0 °C. A solution of boron tribromide (4.4 mL, 1.0 M solution in dichloromethane) was added carefully to the stirred solution under a nitrogen atmosphere. After 4 h, the reaction mixture was cooled and then hydrolyzed by careful shaking with 10 mL of water and extracted twice with 10 mL of dichloromethane. The combined organic phases were then dried over magnesium sulfate, filtered, and evaporated in vacuo, and the crude product was purified by silica gel column chromatography with ethyl acetate/*n*-hexane (1/1) as eluent to afford **1g**: yellow solid; yield 260 mg (91%); mp 224−225 °C; ^{1}H NMR (400 MHz, CD_2Cl_2, ppm) 15.11 (s, 1H), 8.29 (d, J = 2.2 Hz, 1H), 8.18 (dd, J_1 = 9.1 Hz, J_2 = 2.2 Hz, 1H), 7.12 (s, 1H), 7.01 (d, J = 9.1 Hz, 1H), 3.24 (s, 3H), 2.44 (s, 3H); ^{13}C NMR (100 MHz, CD_2Cl_2, ppm) 167.2, 164.0, 159.5, 140.2, 134.2, 132.0, 128.6, 127.4, 120.1, 119.6, 26.9, 15.3; MS (EI, 70 eV) m/z (relative intensity) 261 (M^+, 100); HRMS calcd for $C_{12}H_{11}O_4N_3$ 261.0750, found 261.0748. Anal. Calcd for $C_{12}H_{11}O_4N_3$: C, 55.17; H, 4.24; N, 16.09. Found: C, 55.01; H, 4.22; N, 16.35. Yellow needle-shaped crystals suitable for the crystallographic studies reported here were isolated over a period of 6 weeks by slow evaporation from the chloroform solution.

*4.2.19. (Z)-4-((1H-Pyrrol-2-yl)methylene)-1-methyl-2-phenyl-1H-imidazol-5(4H)-one (**1h-Z**).* (*Z*)-4-((1*H*-Pyrrol-2-yl)methylene)-2-phenyloxazol-5(4*H*)-one[12] (**2h-Z**; 1.0 g, 4.2 mmol) was added to potassium carbonate (0.6 g, 4.3 mmol) in a 50 mL round-bottom flask, in which 20 mL of ethanol (95%) and 1.0 mL of methylamine (40% aqueous) were then added. The reaction mixture was refluxed for 3 h. After cooling, the mixture was neutralized with 10% HCl and extracted with CH_2Cl_2 (3 × 25 mL). After solvent was removed, the crude product was purified by silica gel column chromatography with ethyl acetate/*n*-hexane (1/3) as eluent to afford **1h-Z**: yellow solid; yield 0.69 g (65%); mp 183−184 °C; ^{1}H NMR (400 MHz, CD_2Cl_2, ppm) 11.12 (br, 1H), 7.79 (m, 2H), 7.57 (m, 3H), 7.18 (s, 1H), 7.11(s, 1H), 6.69 (s, 1H), 6.31 (dd, J_1 = 6.0 Hz, J_2 = 2.8 Hz, 1H), 3.39 (s, 3H); ^{13}C NMR (100 MHz, CD_2Cl_2, ppm) 170.2, 158.5, 133.5, 131.0, 129.7, 129.4, 128.8, 128.4, 125.7, 119.3, 118.8, 111.1, 28.8; MS (EI, 70 eV) m/z (relative intensity) 251 (M^+, 100); HRMS calcd for $C_{15}H_{13}ON_3$ 251.1059, found 251.1058. Anal. Calcd for $C_{15}H_{13}ON_3$: C, 71.70; H, 5.21; N, 16.72. Found: C, 71.42; H, 5.27; N, 16.98.

*4.2.20. (E)-4-((1H-Pyrrol-2-yl)methylene)-1-methyl-2-phenyl-1H-imidazol-5(4H)-one (**1h-E**).* (*E*)-4-((1*H*-Pyrrol-2-yl)methylene)-2-phenyloxazol-5(4*H*)-one[12] (**2h-E**; 1.0 g, 4.2 mmol) was added to potassium carbonate (0.6 g, 4.3 mmol) in a 50 mL round-bottom flask, in which 20 mL of ethanol (95%) and 1.0 mL of methylamine (40% aqueous) were then added. The reaction mixture was refluxed for 3 h. After cooling, the mixture was neutralized with 10% HCl and extracted with CH_2Cl_2 (3 × 25 mL). After solvent was removed, the crude product was purified by silica gel column chromatography with ethyl acetate/*n*-hexane (1/3) as eluent to afford **1h-E**: yellow solid; yield 0.64 g (61%); mp 196−197 °C; ^{1}H NMR (400 MHz, CD_2Cl_2, ppm) 13.21 (br, 1H), 7.76 (m, 2H), 7.55 (m, 3H), 7.37 (s, 1H), 7.19 (s, 1H), 6.79 (s, 1H), 6.41 (dd, J_1 = 5.2 Hz, J_2 = 2.0 Hz, 1H), 3.41 (s, 3H); ^{13}C NMR (100 MHz, CD_2Cl_2, ppm) 169.2, 155.4, 132.7, 130.6, 129.5, 129.4, 128.8, 128.2, 128.0, 125.8, 121.3, 112.2, 29.1; MS (EI, 70 eV) m/z (relative intensity) 251 (M^+, 100); HRMS calcd for $C_{15}H_{13}ON_3$ 251.1059, found 251.1054. Anal. Calcd for $C_{15}H_{13}ON_3$: C, 71.70; H, 5.21; N, 16.72. Found: C, 71.52; H, 5.25; N, 16.90. Yellow needle-shaped crystals suitable for the crystallographic studies reported here were isolated over a period of 6 weeks by slow evaporation from the chloroform solution.

4.3. Measurements. Steady-state absorption and emission spectra were recorded with an UV−vis spectrophotometer and a fluorometer, respectively. Quinine sulfate with an emission yield of $\Phi \approx 0.54 \pm 0.02$ in 1.0 N sulfuric acid solution served as the standard to calculate the emission quantum yield. An integrating sphere was applied to measure the quantum yield in the solid state, for which the solid thin film was prepared via direct vacuum deposition and was excited by an argon ion laser at ∼363 nm. The resulting luminescence was acquired with an intensified charge-coupled detector for subsequent quantum yield analyses according to a reported method.[17]

A detailed setup of femtosecond dynamical measurements has been elaborated in our previous report.[18] Briefly, the fundamental of a Ti:sapphire laser at 750−840 nm (80 MHz, 120 fs) was used to produce second harmonics (SH) at 375−420 nm. The resulting fluorescence and the optical delayed remaining fundamental pulses were collected and focused on a BBO type I crystal (0.5 mm) for the sum−frequency generation. The upconversion signal was then separated and detected via a photon counting PMT. The cross correlation between SH and the fundamental had a full width at half-maximum (fwhm) of 220 fs, which was chosen as a response function of the system. A half-wave plate was placed in the pump beam path to ensure that the polarization of the pump laser was set at the magic angle (54.78°) with respect to that of the probe laser to eliminate the fluorescence anisotropy. For picosecond lifetime measurements, a time-correlated single photon counter (TCSPC) was used as a detecting system. The excitation source was similar to that for the femtosecond dynamic measurements by using SH of the Ti:sapphire laser. The fundamental pulse was used as the trigger signal to synchronize TCSPC. The resolution of the time-correlated photon counting system is limited by the detector response of ∼30 ps. The fluorescence decays were analyzed by the sum of exponential functions

dx.doi.org/10.1021/jo2012384 | J. Org. Chem. 2011, 76, 8189−8202

with an iterative convolution method.[18] The solid-state emission was collected >45° from the pump beam to avoid the scattering line reflecting from the sample surface. The solid film was prepared using vacuum deposition on quartz for uniform and homogeneous surface properties.

4.4. Theoretical Approach. To gain further insight into the experimental evidence, the basis set HF/6-31++G(d′,p′) was used to obtain the ground-state geometries of each species and their tautomerized forms.[19] Each minimum was checked by frequency analysis to confirm that the number of imaginary frequencies is 0. On the basis of the HF-optimized geometries, TDB3LYP/6-31++G(d′,p′) was used to access the vertical excitation energies of each species and their tautomerized forms.[20] All calculations were done with the Gaussian 03 program.[21] In addition, on the basis of the time-dependent DFT method (TDDFT/B3LYP/cc-pVDZ and aug-cc-pVDZ) implemented in the TURBOMOLE 5.8 software package,[22] we also carried out the geometry relaxation after Franck−Condon excitation to examine the feasibility of ESIPT in a qualitative manner.

4.5. Fabrication of OLEDs. OLEDs were fabricated by vacuum deposition of the materials at 10^{-6} Torr onto ITO-coated glass substrates having a sheet resistance of 15 Ω square^{-1}. The ITO surface was cleaned through ultrasonication sequentially with acetone, methanol, and deionized water, followed by treatment with UV−ozone. A hole-injection layer of PEDOT:PSS was spin-coated onto the substrates and dried at 130 °C for 30 min to remove residual water. Organic layers were then vacuum-deposited at a deposition rate of ca. 1−2 Å s^{-1}. Subsequently, LiF was deposited at 0.1 Å s^{-1} and then capped with Al (ca. 5 Å s^{-1}) by shadow masking without breaking the vacuum. The current−voltage−brightness (*I*−*V*−*L*) characteristics of the devices were measured simultaneously using a Keithley 6430 source meter and a Keithley 6487 picoammeter equipped with a calibration Si-photodiode. EL spectra were measured using an Ocean Optics spectrometer.

■ ASSOCIATED CONTENT

Ⓢ Supporting Information

Figures, tables, text, and CIF files giving ^{1}H and ^{13}C NMR spectra of the synthesized compounds, X-ray crystallography data for **1a**−**e**,**g** and **1h**-*E*, EL performances of the device (**1a**), and theoretical studies. This material is available free of charge via the Internet at http://pubs.acs.org.

■ AUTHOR INFORMATION

Corresponding Author

*K.-Y.C.: e-mail, kyuchen@fcu.edu.tw; tel, +886-4-2451-7250; fax, +886-4-2451-0890. W.-Y.H.: e-mail, wenhung@mail.ntou.edu.tw; tel, +886-2-2462-2192 ext. 6718; fax, + 886-2-2463-4360. P.-T.C.: email, chop@ntu.edu.tw; tel, +886-2-3366-3894; fax, +886-2-2369-5208.

■ ACKNOWLEDGMENTS

We thank the National Science Council (Grant No. 99-1989-2004) for financial support. We are also grateful to the National Center for High-Performance Computing of Taiwan for allowing us generous amounts of computing time.

■ REFERENCES

(1) (a) Chalfie, M.; Tu, Y.; Euskirchen, G.; Ward, W. W.; Prasher, D. C. *Science* **1994**, *263*, 802. (b) Lippincott-Schwartz, J.; Patterson, G. H. *Science* **2003**, *300*, 87. (c) Ormo, M.; Cubitt, A. B.; Kallio, K.; Gross, L. A.; Tsien, R. Y.; Remington, S. J. *Science* **1996**, *273*, 1392. (d) Zimmer, M. *Chem. Rev.* **2002**, *102*, 759. (e) Tsien, R. Y. *Annu. Rev. Biochem.* **1998**, *67*, 509. (f) Matz, M. V.; Fradkov, A. F.; Labas, Y. A.; Savitsky, A. P.; Zaraisky, A. G.; Markelov, M. L.; Lukyanov, S. A. *Nat. Biotechnol.* **1999**, *17*, 969. (g) Hastings, J. W.; Morin, J. G., In *Green Fluorescent Protein*; Chalfie, M., Kain, S., Eds.; Wiley-Liss: New York, 1998; pp 17−41. (h) Sullivan, K. F.; Kay, S. A. *Green Fluorescent Proteins*; Academic Press: San Diego, CA, 1999. (i) Chalfie, M. *Green Fluorescent Proteins, Properties, Applications and Protocols*; Wiley-Liss: New York, 1998.

(2) (a) Agmon, N. *Biophys. J.* **2005**, *88*, 2452. (b) Stoner-Ma, D.; Jaye, A. A.; Matousek, P.; Towrie, M.; Meech, S. R.; Tonge, P. J. *J. Am. Chem. Soc.* **2005**, *127*, 2864. (c) Hosoi, H.; Mizuno, H.; Miyawaki, A.; Tahara, T. *J. Phys. Chem. B* **2006**, *110*, 22853.

(3) (a) Stoner-Ma, D.; Melief, E. H.; Nappa, J.; Ronayne, K. L.; Tonge, P. J.; Meech, S. R. *J. Phys. Chem. B* **2006**, *110*, 22009. (b) Abbyad, P.; Childs, W.; Shi, X.; Boxer, S. G. *Proc. Natl. Acad. Sci. U.S.A.* **2007**, *104*, 20189. (c) Stoner-Ma, D.; Jaye, A. A.; Ronayne, K. L.; Nappa, J.; Meech, S. R.; Tonge, P. J. *J. Am. Chem. Soc.* **2008**, *130*, 1227. (d) Fang, C.; Frontiera, R. R.; Tran, R.; Mathies, R. A. *Nature* **2009**, *462*, 200.

(4) (a) Brejc, K.; Sixma, T. K.; Kitts, P. A.; Kain, S. R.; Tsien, R. Y.; Ormo, M.; Remington, S. J. *Proc. Natl. Acad. Sci. U.S.A.* **1997**, *94*, 2306. (b) Litvinenko, K. L.; Webber, N. M.; Meech, S. R. *J. Phys. Chem. A* **2003**, *107*, 2616. (c) Mandal, D.; Tahara, T.; Meech, S. R. *J. Phys. Chem. B* **2004**, *108*, 1102. (d) Usman, A.; Mohammed, O. F.; Nibbering, E. T. J.; Dong, J.; Solntsev, K. M.; Tolbert, L. M. *J. Am. Chem. Soc.* **2005**, *127*, 11214. (e) Dong, J.; Solntsev, K. M.; Tolbert, L. M. *J. Am. Chem. Soc.* **2006**, *128*, 12038.

(5) He, X.; Bell, A. F.; Tonge, P. J. *Org. Lett.* **2002**, *4*, 1523.

(6) Schaefer, T. *J. Phys. Chem.* **1975**, *79*, 1888.

(7) (a) Stavrov, S. S.; Solntsev, K. M.; Tolbert, L. M.; Huppert, D. *J. Am. Chem. Soc.* **2006**, *128*, 1540. (b) Gepshtein, R.; Huppert, D.; Agmon, N. *J. Phys. Chem. B* **2006**, *110*, 4434. (c) Usman, A.; Mohammed, O. F.; Nibbering, E. T. J.; Dong, J.; Solntsev, K. M.; Tolbert, L. M. *J. Am. Chem. Soc.* **2005**, *127*, 11214.

(8) (a) Webber, N. M.; Litvinenko, K. L.; Meech, S. R. *J. Phys. Chem. B* **2001**, *105*, 8036. (b) Polyakov, I. V.; Grigorenko, B. L.; Epifanovsky, E. M.; Krylov, A. I.; Nemukhin, A. V. *J. Chem. Theory Comput.* **2010**, *6*, 2377.

(9) (a) Dong, J.; Solntsev, K. M.; Poizat, O.; Tolbert, L. M. *J. Am. Chem. Soc.* **2007**, *129*, 10084. (b) Solntsev, K. M.; Poizat, O.; Dong, J.; Rehault, J.; Lou, Y.; Burda, C.; Tolbert, L. M. *J. Phys. Chem. B* **2008**, *112*, 2700. (c) Baldridge, A.; Feng, S.; Chang, Y.-T.; Tolbert, L. M. *ACS Comb. Sci.* **2011**, *13*, 214.

(10) Chen, K. Y.; Cheng, Y. M.; Lai, C. H.; Hsu, C. C.; Ho, M. L.; Lee, G. H.; Chou, P. T. *J. Am. Chem. Soc.* **2007**, *129*, 4534.

(11) Hsieh, C. C.; Chou, P. T.; Shih, C. W.; Chuang, W. T.; Chung, M. W.; Lee, J.; Joo, T. *J. Am. Chem. Soc.* **2011**, *133*, 2932.

(12) (a) Rao, Y. S.; Filler, R. *Synthesis* **1975**, *12*, 749. (b) Sidhu, G. S.; Venkataratnam, R. V.; Prasad, K. K.; Iyengar, D. S. *Indian J. Chem.* **1972**, *10*, 448.

(13) (a) Siebrand, W. *J. Chem. Phys.* **1967**, *47*, 2411. (b) Chen, K. Y.; Hsieh, C. C.; Cheng, Y. M.; Lai, C. H.; Chou, P. T. *Chem. Commun.* **2006**, 4395.

(14) You, Y.; He, Y.; Burrows, P. E.; Forrest, S. R.; Petasis, N. A.; Thompson, M. E. *Adv. Mater.* **2000**, *12*, 1678.

(15) Shin, M. G.; Thangaraju, K.; Kim, S. O.; Park, J. W.; Kim, Y. H.; Kwon, S. K. *Org. Electron.* **2011**, *12*, 785.

(16) (a) Ma, D.; Liang, F.; Wang, L.; Lee, S. T.; Hung, L. S. *Chem. Phys. Lett.* **2002**, *358*, 24. (b) Kim, S.; Seo, J.; Jung, H. K.; Kim, J. J.; Park, S. Y. *Adv. Mater.* **2005**, *17*, 2077. (c) Gaenko, A. V.; Devarajan, A.; Tselinskii, I. V.; Ryde, U. *J. Phys. Chem. A* **2006**, *110*, 7935. (d) Park, S.; Kwon, J. E.; Kim, S. H.; Seo, J.; Chung, K.; Park, S. Y.; Jang, D. J.; Medina, B. M.; Gierschner, J.; Park, S. Y. *J. Am. Chem. Soc.* **2009**, *131*, 14043. (e) Kim, S. H.; Park, S.; Kwon, J. E.; Park, S. Y. *Adv. Funct. Mater.* **2011**, *21*, 644. (f) Yao, D.; Zhao, S.; Guo, J.; Zhang, Z.; Zhang, H.; Liu, Y.; Wang, Y. *J. Mater. Chem.* **2011**, *21*, 3568.

(17) de Mello, J. C.; Wittmann, H. F.; Friend, R. H. *Adv. Mater.* **1997**, *9*, 230.

(18) Chou, P. T.; Chen, Y. C.; Yu, W. S.; Chou, Y. H.; Wei, C. Y.; Cheng, Y. M. *J. Phys. Chem. A* **2001**, *105*, 1731.

(19) Petersson, G. A.; Al-Laham, M. A. *J. Chem. Phys.* **1991**, *94*, 6081.

(20) (a) Bauemschmitt, R.; Ahlrichs, R. *Chem. Phys. Lett.* **1996**, *256*, 454. (b) Casida, M. E.; Jamorski, C.; Casida, K. C.; Salahub, D. R. *J. Chem. Phys.* **1998**, *108*, 4439.

(21) Frisch, M. J.; Trucks, G. W.; Schlegel, H. B.; Scuseria, G. E.; Robb, M. A.; Cheeseman, J. R.; Montgomery, J. A. Jr.; Vreven, T.; Kudin, K. N.; Burant, J. C.; Millam, J. M.; Iyengar, S. S.; Tomasi, J.; Barone, V.; Mennucci, B.; Cossi, M.; Scalmani, G.; Rega, N.; Petersson, G. A.; Ehara, M.; Toyota, K.; Hada, M.; Fukuda, R.; Hasegawa, J.; Ishida, M.; Nakajima, T.; Kitao, O.; Nakai, H.; Honda, Y.; Nakatsuji, H.; Li, X.; Knox, J. E.; Hratchian, H. P.; Cross, J. B.; Adamo, C.; Jaramillo, J.; Cammi, R.; Pomelli, C.; Gomperts, R.; Stratmann, R. E.; Ochterski, J.; Ayala, P. Y.; Morokuma, K.; Salvador, P.; Dannenberg, J. J.; Zakrzewski, V. G.; Dapprich, S.; Daniels, A. D.; Strain, M. C.; Farkas, O.; Malick, D. K.; Rabuck, A. D.; Raghavachari, K.; Foresman, J. B.; Ortiz, J. V.; Cui, Q.; Baboul, A. G.; Clifford, S.; Cioslowski, J.; Stefanov, B. B.; Liu, G.; Liashenko, A.; Piskorz, P.; Komaromi, I.; Martin, R. L.; Fox, D. J.; Keith, T.; Al-Laham, M. A.; Peng, C. Y.; Nanayakkara, A.; Challacombe, M.; Gill, P. M. W.; Johnson, B.; Chen, W.; Wong, M. W.; Gonzalez, C.; Pople, J. A. *Gaussian 03, version A.1*; Gaussian, Inc., Pittsburgh, PA, 2002.

(22) Ahlrichs, R.; Bar, M.; Haser, M.; Horn, H.; Kolmel, C. *Chem. Phys. Lett.* **1989**, *162*, 165.